Peer-reviewed version available at Minerals 2018, 8, 585; doi:10.3390/min8120585

Article

The extracellular and intracellular biomineralization induced by *Bacillus licheniformis* DB1-9 at different Mg/Ca molar ratios.

Zuozhen Han[1, 2*], Xiao Gao[1], Hui Zhao[1, 3], Maurice E. Tucker[4,5], Yanhong Zhao[1], Huaxiao Yan[1,3*]

[1] Shandong Provincial Key Laboratory of Depositional Mineralization and Sedimentary Minerals, College of Earth Science and Engineering, University Hospital, Shandong University of Science and Technology, Qingdao, 266590, China
[2] Laboratory for Marine Mineral Resources, Qingdao National Laboratory for Marine Science and Technology, Qingdao, 266237, China
[3] Department of Bioengineering, College of Chemical and Environmental Engineering, Shandong University of Science and Technology, 266590, Qingdao, P. R. China
[4] School of Earth Sciences, University of Bristol, Bristol, BS8 1RJ, UK
[5] Cabot Institute, University of Bristol, Cantock's Close, Bristol, BS8 1UJ, UK
✉: Zuozhen Han; Tel.: +86 532 86057286; E-mail: hanzuozhen65@126.com
✉: Huaxiao Yan; Tel.: +86 532 86057625; E-mail: 15954804511@163.com
Zuozhen Han, Xiao Gao and Hui Zhao as the co-first authors.

Abstract: Biomineralization has become a research hotspot and attracted widespread attention in the field of carbonate sedimentology. In this study, *Bacillus licheniformis* DB1-9 was used to induce the calcium carbonate precipitation at different magnesium calcium molar ratios in the laboratory to further explore the biomineralization mechanism. Phylogenetic tree shows that the bacteria belongs to *Bacillus licheniformis* species. The ammonia and carbonic anhydrase can be released by this bacteria, resulting in the pH increase, and the carbonic anhydrase can also promote the hydration reaction of carbon dioxide and subsequently produce the bicarbonate and carbonate ions to elevate the supersaturation of calcium carbonate in the liquid culture medium to facilitate the precipitation of carbonate minerals. The calcites have a shape of rhombohedron, dumbell, and elongation, and aragonite often appears in the form of mineral aggregates, besides that there are also the spherical and the fusiform minerals. FTIR result shows there are some organic functional groups, such as C-O-C and C=O, beside of the characteristic peaks of the calcite and the aragonite, indicating that microbial metabolism is closely related to the mineral formation. The superthin slices of the bacteria analyzed by HRTEM, SAED, EDS and STEM show that the surface and EPS can adsorb a large number of calcium ions and magnesium ions and EPS may act as the nucleation sites, what's more, the intracellular nanometer-scale sphere areas show the amorphous structures, and the intracellular calcium ions and magnesium ions suggeste that they can be transported from the outside to inside the cell by diffusion along the concentration grade from high to low. This study may provide some references to further understand the biomineralization mechanism induced by microorganisms in the laboratory and the field, and also helps to explore the reason of the transition of calcite sea to aragonite sea in the geological history.

keywords: Mg/Ca; biominerliazation; nucleation site; *Bacillus licheniformis* DB1-9; carbonic anhydrase; ammonia

1. Introduction

The Cambrian explosion is one of the most important event in the evolution of life. In the Cambrian period, a large number of microbialites were developed, in which the fossilized cyanobacteria were preserved [1, 2]. Carbonates in sedimentary rocks usually as good oil and gas

reservoirs [3-7], in which many traces of microorganisms have also been discovered. Cyanobacteria act as the "skeleton" in the microbialites and have played an important role in the formation of microbialites. In order to further explore the formation process of microbialites [8-13] and rebuild the survival environment, many researchers have performed experiments by using different species of cyanobacteria to induce carbonate minerals in the laboratory and the field [14-20]. Some researchers have investigated the formation mechanism of in situ calcified stromatolites in the natural environments. For example, *Kempe and Kazmierczak, 1990* have reported that the in situ calcified stromatolites can be induced by the spherical cyanobacteria; the lamellar stromatolites can be formed between the adjacent cyanobacteria mats in a modern marine coral reefs in Bahamas, and the calcification process also occurs to the living cyanobacteria (*Dichothrix* sp.) by photosynthesis [14]. Some people have also studied the mineralogy of the carbonates induced by various cyanobacteria: a freshwater cyanobacterium *Synechococcus* PCC 7942 can accelerate the dissolution of the silicate and promote the nucleation and sedimentation of magnesium carbonate at the ambient temperatures [16]; Power et al. have found that the filamentous cyanobacteria (*Lyngbya* sp.) can induce dypingite and aragonite [20]; the calcium carbonate on the surface and edge of cyanobacteria *Gloeocapsa* sp. is finally determined as calcite [17]; calcite can also be induced by *Synechocystis* sp. PCC6803 cyanobacteria at different Ca^{2+} concentrations, Mg-calcite at lower Mg/Ca molar ratios and aragonite at higher Mg/Ca molar ratios [22-27]. Of course, the biomineralization induced by the cyanobacteria not only takes place outside the cell, but also inside the cell and on the cell surface. Recently, *Cam et al.* have collected the stromatolites from the volcanic lake of Alchichica in Mexico and cultured them in the laboratory and isolated a new species of cyanobacteria (*Candidatus Gloeomargarita* lithophora) and found that the physiological and biochemical activities of cyanobacteria can involve in the intracellular biomineralization process [15]. The research result reported by *Cam et al.* can help us to further understand the formation mechanism of intracellular carbonates of the cyanobacteria. The biomineralization on the surface of cyanobacteria is complicated. The amorphous or nano-meter calcium carbonate nucleated on the extracellular polymers (EPS) of *Gloeocapsa leopoliensis* PCC 7942 has been determined as the transitional precursor of the calcite, suggesting that the amorphous calcium carbonate (ACC) may act as a “helper” to protect the cyanobacteria from suffering from the precipitation coming from the formation of the uncontrolled thermodynamically stable calcite [18]. Martinez et al. have reported that the *Planktothrix* sp. and *Synechococcus* sp. cyanobacteria can maintain the positive charge properties of the surface, thereby protecting the cyanobacteria from the adsorbtion of calcium ions and the precipitation of carbonate on the surface [19]. However, there are also inconsistencies. *Synechocystis* sp. PCC6803 cyanobacteria can be wrapped by calcite at different Ca^{2+} concentrations [22-27]. In summary, many scholars have used variety of cyanobacteria to carry out numerous research work to investigate the biomineralization mechanism. While due to the abundant species of the bacteria, other bacteria except the cyanobacteria should also be used to do some research work to help the further exploration of the biomineralization mechanism.

Experiments on the induction of minerals by heterotrophic bacteria have also been carried out. Many researchers have performed experiments to induce carbonates precipitation by halophiles due to the fact that the salinity has been considered to be a key factor in the process of biomineralization. The dolomite was precipitated mediated by *Haloferax volcanii* DS52 under a high salinity, and the water molecules adsorbed around the magnesium ions may be a kinetic barrier to affect the biomineralization of the magnesium ions [28]. The *Chromohalobacter israelensis* LD532 bacteria were used to inudce the Mg-rich calcite and aragonite minerals under a lower salt condition and the special organic functional group such as C-O-C and –OH maybe had a close relationship with the biominerlization process [29]. *Halobacillus trueperi* bacteria were chosen to induce minerals at different salt concentrations and played an important role in the carbonate precipitation [30]. Both sulfate-reducing bacteria (SRB) and halophilic bacteria were successfully used to induce the formation of dolomite by Deng et al. and the bacterial EPS were proved to act as the nucleation site of the dolomite [31]. Besides of the halophiles, the famous SRB and methanogenic Archaea have also been used to do some experiments about biomineralization, which

also makes great contribution to the deep understanding of the biomineralization mechanism. *Acinetobacter calcoaceticus SRB4* has been used to induce the struvite, a kind of phosphate mineral [32], and the EPS could be considered as the nucleation site. *Braissant et al.* have found that the EPS extractd from *Desulfovibrio H0407_12.1Lac* have a strong capacity to adsorb metal ions [33]. Mg-calcite and Ca-dolomite has also been formed in the presence of EPS produced by SRB [34], indicating that the EPS play an important role in the biomineralization process. The low-temperature dolomite from an anaerobic microbial consortium can also be precipitated in the presence of the methanogenic Archaea [35], indirectly suggesting that the microbes that induce dolomite are diverse. Meanwhile, some scholars have also conducted research work on biomineralizaiton induced by some other aerobic bacteria. The dolomite could also be induced by *Virgibacillus marismortui* and *Marinobacter sp.* in the presence of oxygen [36]. The spherical vaterite was induced by *Lysinibacillus* sp. strain GW-2, which was usually considered as the unstable mineral in the past and finally could transformed into calcite, and the biogenetic vaterite was more stable than the chemically derived minerals [37]. It has been reported that *Myxococcus* sp. bacteria had a ability to induce various minerals, including phosphates, carbonates, sulfates, chlorides, oxalates and silicates [38]. However, the factors controlling the bacterial biomineralization are not specific due to the complicated bacterial metabolic activities [38]. The *Myxococcus xanthus* could promote the calcite growth, menahwhile, the stress resistant ability of biogenetic calcite was stronger than that of the chemical calcite [39]. Some researchers have reported that the carbonate induced by the marine bacteria was affected by the medium viscosity, the calcite was formed at a slow ion diffusion rate and the aragonite was precipitated under the condition of a quick ion diffusion rate [40]. To sum up, many different types of microorganisms have been widely used to induce minerals, and in-depth research has been conducted on exploration the biomineralization mechanism of different microorganisms, and many innovative conclusions have also been obtained, but there are still many unsolved problems.

There are some controversial topics in the process of biomineralization induced by microorganisms. Some researchers have believed that the spherulite and dumbbell shape of the minerals could be considered as an important characteriatics to judge the microbial origin [40], however there are some disagreements on this opinion: the spherical mineral can also be precipitated in the liquid culture medium without inoculation of bacteria [41], maybe due to the existence of organic substaces such as tryptone and beef extract; minerals with such structures have also been obtained by Sanchez-Roman et al. in the abiotic condition [36]; other researchers have believed that the spherical minerals are formed not only by biological factors, but also by organic substances, and even in the inorganic environment [31, 42]. A large number of references have been reported that pH increase is beneficial to the elevation of supersaturation in the environment to promote the precipitation of minerals and ammonia released by the bacteria was the main reason to cause pH increase [42-44]. The idea that pH increase is caused mainly by ammonia has been accepted by almost all the researchers for many years. However, other researchers disagree with the opinion recently and reported that some microbes could not produce enough ammonia to increase the pH to a level close to or even above 9, there should be other factors to afffect the pH increase, and carbonic anhydrase (CA) could promote the hydration reaction of carbon dioxide to release bicarbonate and carbonate ions, which could also increase pH values with the help of ammonia [41]. Some scholars have also believed that the bacterial cell surface provides a nucleation site [26], however, others have thought that EPS provides a nucleation site [45-47]. There is also some controversies about the nucleation mechanism: some researchers have concluded that the acidic amino acids such as aspartic acid (Asp) and glutamic acid (Glu) play an important role [48, 49]; meanwhile, some scholars have believed that the combined effect of proteins and polysaccharides also take part in the process [46, 50]; others have affirmed that certain specific organic functional groups and gene sequences regulate the formation of crystals [46, 50]. Therefore, the research work on the nucleation site and the nucleation mechanism is needed to further explore. The biomineralization of minerals induced by microorganism should include the intracellular and extracellular biomineralization parts [51]. Many researchers have aimed at the extracellular

biomineralization, namely the morphology and mineralogy of the microbially induced mineral and the extracellular biomineralization mechanism, always neglected and omited the intracellular biomineralization part. At present, only a few researchers in the world are studying the intracellular biomineralization part: *Candidatus Gloeomargarita* lithophora, a new cyanobacterial species, has been found to contain the intracellular amorphous carbonates (nanospheres) [52]; cyanobacterial intracellular biomineralization have also been studied by *Benzerara et al.* and they have found that different species of cyanobacteria can form the different numbers of inclusions (nanospheres) per cell [53]. *Perri et al., 2017* have reported that the intracellular nanospheres induced by microorganisms in the biomineralization process have generally been considered as the mineralized bacterial vesicles or viruses [120]. In my opinion, the intracellular biomineralization is also very interesting and should be as a indivisible part in the whole research work.

Based on this, we have performed the experiment to expect to obtain some valuble results about the spherical mineral, the reason of the pH increase, the nucleation site and the nucleation mechanism, and the intresting intracellular biomineralization. In this paper, five different grades of Mg/Ca molar ratios (0, 3, 6, 9, 12) have been set to investigate the biomineralization process and mechanism induced by *Bacillus licheniformis* DB1-9 bacteria. In this study, a phylogenetic tree of the DB1-9 bacteria was established using the neighbor-joining method, the bacterial growth curve and pH curve, the carbonic anhydrase (CA) activities, the carbonate and bicarbonate concentrations, and ammonia test were also investigated to explore the formation mechanism of the minerals induced by the bacteria, the mineralogy, morphology, element composition, and the organic functional groups of the minerals at different Mg/Ca ratios were also detected by XRD, SEM-EDS and FTIR. In order to further investigate the intracellular biomineralization, the superthin slices of the bacteria were prepared and studied by HRTEM, SAED, EDS and STEM. Through a series of experiments in the laboratory, the biomineralization mechanism may be modified and supplemented. This study may provide some references to further understand the biomineralization mechanism induced by microorganisms in the laboratory and the field, and also helps to explore the reason of the transition of calcite seas to aragonite seas in the geological history.

2.Materials and methods

2.1 Identification of DB1-9 Bacteria and the Preparation of the Liquid Seed.

The bacteria DB1-9 was presented by associate professor Huaxiao Yan in the department of bioengineering, which has been preserved in a refrigerator at -20 °C. According to the methods published before [24, 25, 32, 41], the total DNA of the bacteria DB1-9 was extracted and used as the template to amplify the 16S rDNA, and then the sequences of 16S rDNA were sequenced by Shanghai Sangon Biotech Co., Ltd (Shanghai,China). The complete DNA sequences were obtained through fragment assembly using DNAMAN 8.0 software and uploaded to the Genbank, and then the Basic Local Alignment Search Tool (BLAST) was used to compare the nucleotide homology between the 16S rDNA of bacteria DB1-9 and those of other bacteria registrated in the Genbank. The phylogenetic tree of DB1-9 was established with neighbor-joining method by MEGA 7.0 software [51].

The culture medium for activation and multiplication culture of DB1-9 bacteria contains the following ingredients (per L): beef extract 5.0 g, NaCl 5.0 g, tryptone 10.0 g, pH 7.0. The solid culture medium was prepared by adding 20 g of agar powder based on the above components. A single colony of DB1-9 bacteria was selected and inoculated into the liquid culture medium to culture about 24h at 30 °C in a constant temperature oscillation incubator (HZQ-F160, Harbin Donglian Electronic Technology Development Co., Ltd, Longjiang Hei, China) with a speed of 130 rpm. The cell concentrations could be measured by a spectrophotometer (721, Shanghai Aoxi Scientific Instrument Co., LTD, Shanghai, China) at a wavelength of 600 nm. When the OD_{600} was up to 0.8, the preparation of the liquid seed was finished.

2.2 Growth curve, pH Changes, CA Activity and Carbonate and Bicarbonate Concentrations in the Liquid Culture Medium and Ammonia Test.

The liquid seed was inoculated into 500 mL of the sterile liquid culture medium in a 1L conical flask by the volume ratio of 1%. Before 74h, OD_{600} values were measured every 2h by a spectrophotometer; from 74-98h, measured every 6h; finally measured at 98, 128, 146, 162 and 192h. The pH values of the experimental and control group were measured by a pH meter (PB-11, Sartorius, Germany). The CA activity, carbonate and bicarbonate concentrations and ammonia test were detected according to the method described by *Zhuang et al.* [41]. The CA activity was measured every 3h from 0-99h, and then measured at 114, 128 and 152h. The bicarbonate concentrations were measured from 0 to 293h. The carbonate concentration could not be detected before 114 h, therefore, the carbonate concentration was detected in the time range of 114-293 h.

2.3 The Cultivation and Isolation of the Mineral Precipitates.

The liquid culture medium used to cultivate the minerals contains the following ingredients (per L): beef extract 5.0 g, NaCl 5.0 g, tryptone 10.0 g, $CaCl_2$ (0.01 M), Na_2CO_3 (0.006 M), $NaHCO_3$ (0.006 M) and Mg/Ca molar ratio 0, 3, 6, 9 and 12, pH 7.0. Na_2CO_3 and $NaHCO_3$ solution was sterilized by a filter with a 0.22 μm pore-sized membrane. $MgSO_4 \cdot 7H_2O$ (2M) was used to adjust the Mg/Ca molar ratio. The liquid culture medium inoculated with the liquid seed(OD_{600}=0.8) by a volume ratio of 1% was set as the experimental group, and the other group added with the sterile distilled water by the same volume ratio was set as the control group. All the culture was triplicated at each kind of Mg/Ca molar ratio and cultivated in the constant temperature oscillation incubator at 30 °C and with a speed of 130 rpm.

After being cultured for 12d, the precipitates in the experimental group could be observed by the naked eye, and there were no precipitates in the control group. The precipitates in the experimental group were sucked out and transferred into the Eppendorff tube to be washed 3 times with the distilled water, and then preserved in the anhydrous ethanol for future research. After being cultured for 24d, the precipitates in the experimental group were isolated again according to the same method. There were still no precipitates in the control group.

2.4 XRD, FT-IR and SEM-EDX Analyses of Minerals Induced by B. lichniformis DB1-9.

The naturally dried mineral precipitates in the experimental group were analyzed with X-ray diffraction (XRD, D/Max-RC, Japan). The scanning angle (2θ) of XRD ranged from 10° to 90°, with a step size of 0.02° and a count time of 8° min^{-1} [54-58, 59, 60]. The mineral phases of the precipitates were further determined by comparison with the standard data on the powder diffraction file (PDF) of the International Center for Diffraction Data (ICDD) by jade 6.0 software.

The FT-IR (Nicolet 380, Thermo Fisher Scientific Inc., Massachusetts, United States) experiment was conducted by using the potassium bromide method in a scanning range of 400 – 4000cm^{-1} with a resolution of 4 cm^{-1} [61-63].

The minerals in the experimental group were gold-sprayed and analyzed by SEM (S-4800, Hitachi, Tokyo, Japan) [64-69] and at the same time the elemental composition of the minerals were also analyzed by the energy dispersive spectroscop (EDS, EDAX, Mahwah, NJ, USA).

2.5 HRTEM, SAED, STEM Analysis of the Ultrathin Slices of B. lichniformis DB1-9.

The preparation of the superslices of *B. lichniformis* DB1-9 was according to the reference by Han et al., 2017 [24], and the superslices were analyzed by HRTEM (H-7650, Hitachi, Japan) [70-75], STEM (Tecnai G^2 F20, FEI, America) and EDS. The parameters of this instrument were referred to the articles [76-80].

3. Result

3.1 Identification of B. lichniformis DB1-9 Bacteria.

The 16s rDNA sequence of DB1-9 bacteria is 1486 bp and has been uploaded to GenBank and the obtained accession number is MG818748.1. The 16S rDNA of strain DB1-9 shares 99 % homology with 99 strains of *B. licheniformis* by blast in Genbank. The phylogenetic tree based on the 16S rDNA sequence shows that the DB1-9 strain is closest to *B. licheniformis* (Fig. 1), indicating that the DB1-9 strain can be identified as *B. licheniformis* species.

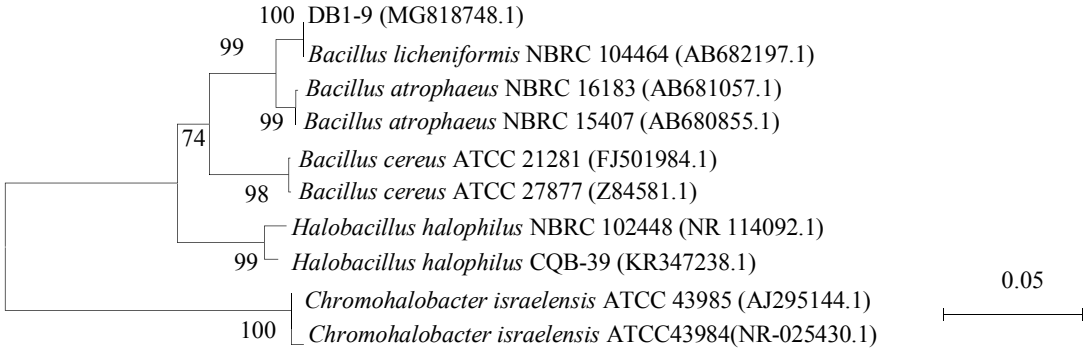

Figure 1. Phylogenetic tree constructed with neighbor-joining method based on bacterial 16S rDNA sequence alignment.

3.2 Growth Curve, pH Curve, CA Activity of DB1-9 bacteria, and Carbonate and Bicarbonate Concentrations in the Culture Medium and the Ammonia Test.

Fig. 2a shows the growth curve of *B. lichniformis* DB1-9 bacteria and the pH curves of the experimental and control group. It can be seen from the growth curve that the adaption phase is from 0-8h, in which the cell concentration increased slowly due to the fact that *B. lichniformis* DB1-9 bacteria needed time to adapt the new environment; the exponential growth period is from 8-46h, the cell concentration increased quickly and the growth rate of *B. lichniformis* DB1-9 bacteria reached to a maximum; the stable phase is from 46-74h, the cell concentration almost kept constant because cells almost stopped reproducing and the growth rate was almost 0; the decline phase is from 74-192h, the cell concentration decreased in this period and the death rate was greater than the birth rate. The growth curve conformed to the general law of microbial growth; however, the pH curve was more interesting than the growth curve. In the adaption phase, pH increases from 6.92 to 7.06; in the exponential growth period, pH sharply increases from 7.06 to 8.25; in the stable phase, pH also increases from 8.25 to 8.6; the most striking thing is that pH continues to rise from 8.6 to 9.27 during the decline phase of *B. lichniformis* DB1-9 bacteria. The released ammonia during the exponential growth period is the reason for pH increase and this idea has been accepted by many reseahers for many years. The ammonia test was performed in the time range of 24-48h, indicating that from 48h, the released ammonia was almost 0. However, pH values were still increasing from 48-192h, suggesting that maybe the released ammonia was not the only reason to cause pH increase, there should be other factors existing in the liquid culture medium which could also cause pH increase. In contrast to the experimental group, the pH value of the control group was almost stable at 7.0, significantly different from that of the experimental goup.

Fig. 2b shows the CA activity of *B. lichniformis* DB1-9 bacteria. It can be obtained that CA activity curve includes two parts: from 0 - 69 h, CA activity increases from 0.145 to 18.682 U/L; from 69–152 h, CA activity decreases from 18.682 to 7.972 U/L. Roughly, the CA change trend was similar to that of the cell growth curve (Fig. 2a): the bacterial concentration increased and at the same time the CA activity also increased; and when the cell concentration decreased the CA activity also decreased. However, CA activity could not decrease to 0, suggesting that even at the decline phase, CA activity still existed in the liquid culture medium. The alkaline CA can promote the hydration

Peer-reviewed version available at Minerals 2018, 8, 585; doi:10.3390/min8120585

reaction of carbon dioxide (CO_2) to produce the bicarbonate and carbonate ions. In this study, when pH increases beyond to 8.0, CA activity still existed, suggesting that CA in this study belonged to

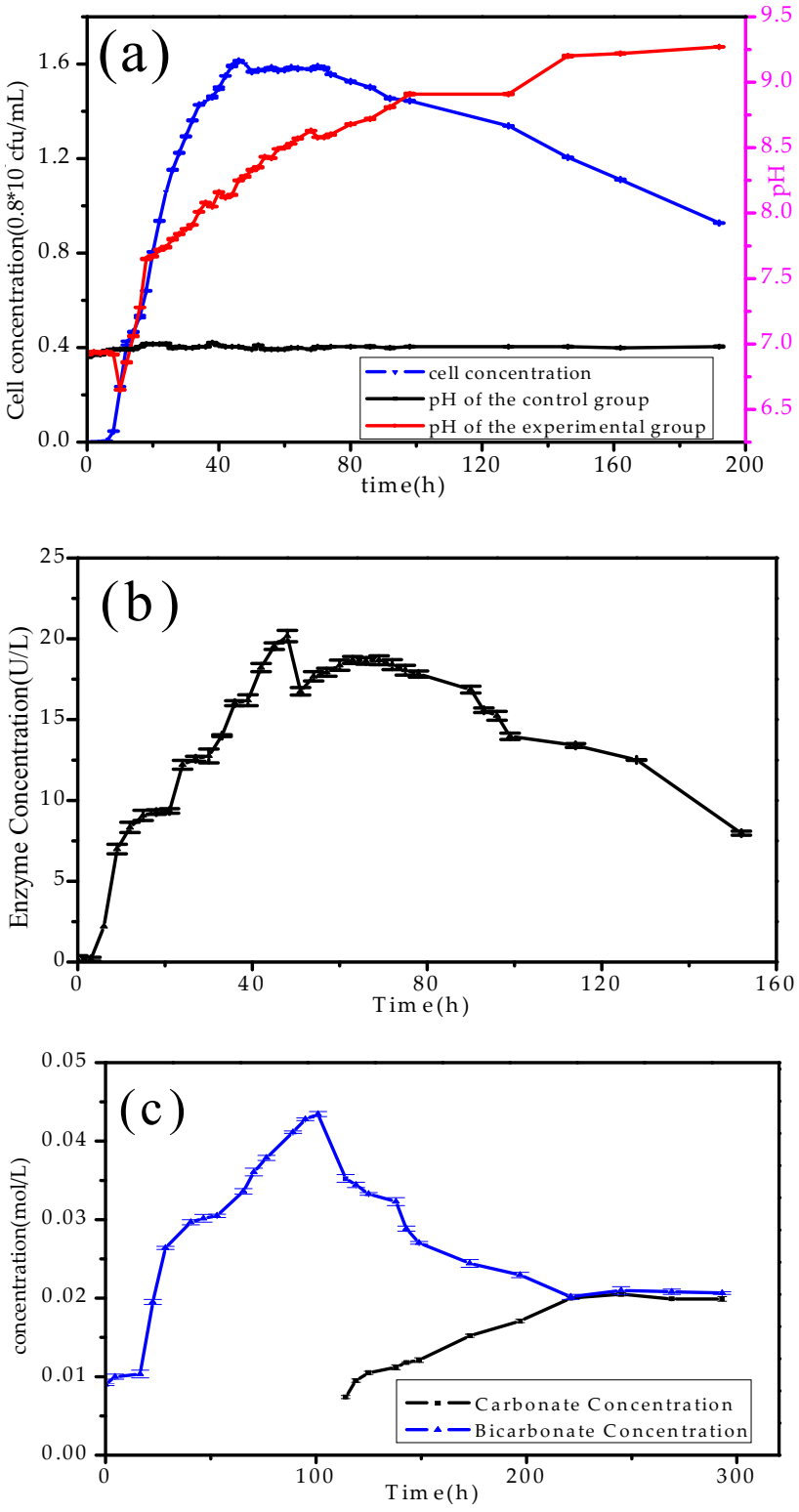

Figure 2. Physiological and biochemical characteristics of *B. lichniformis* DB1-9. (a) The blue line represents the cell growth curve; the red line represents the pH value of the experimental group and the black line represents the pH value of the control group; (b) the curve of CA activity; (c) the curve of carbonate and bicarbonate concentration.

the alkaline CA, and further suggesting that this kind of CA could release the bicarbonate and

Peer-reviewed version available at Minerals 2018, 8, 585; doi:10.3390/min8120585

carbonate ions in our liquid culture medium. Therefore, the bicarbonate and carbonate ion concentrations were also measured in this study.

It is not difficult to found from Fig. 2c that bicarbonate concentration increases from 0.028 - 0.049 M in the time range of 0 – 101 h, and then decreases to 0.0351 M from 101 to 293h; carbonate ion concentration cannot be detected from 0 – 114 h, and increases from 0.0074 to 0.0199 M in the time range of 114-293h. When the bicarbonate concentration decreased, the carbonate ion concentration increased instead, suggesting that the bicarbonate ions occurred the chemical reaction to produce the carbonate ions in the liquid culture medium. The released carbonate ions also promoted the pH increase. Fig. 3 shows that the ammonia can be produced by *B. lichniformis* DB1-9 bacteria because the experimental group shows the dark brown while the control group shows the color of the Nessler's reagent, which also can increase pH increase. That is to say, the pH increase was caused by the combination effect of CA and ammonia released by *B. lichniformis* DB1-9 bacteria.

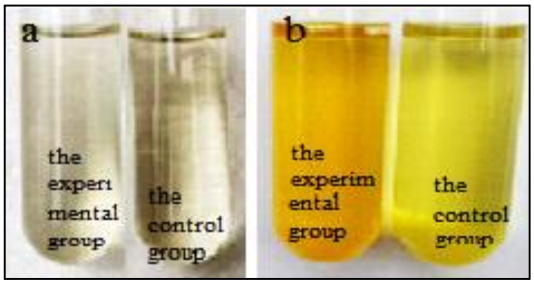

Figure 3. Ammonia test of *B. lichniformis* DB1-9 bacteria.

3.3 XRD Analysis of the Minerals IndIuced by B. lichniformis DB1-9 Bacteria.

Fig. 4 shows that the mineral is calcite at Mg/Ca molar ratio of 0, the mixture of calcite and aragonite at Mg/Ca molar ratio of 3 and only aragonite at Mg/Ca molar ratio of 6, 9, and 12 when the minerals were cultivated for 12 and 24 d. With the cultivation time, 2θ of calcite (104) becomes larger at Mg/Ca molar ratio of 3, that is to say, d(104) of calcite cultivated for 24 d became smaller, indicating that Ca atom could be replaced by Mg atom in the calcite crystal cell and the origial calcite crystal structure was damaged by Mg^{2+} ions. At the same time, the full width at half maximum (FWHM) of calcite (104) at Mg/Ca molar ratio of 3 cultivated for 24 d is larger than that cultivated for 12 d, indicating that the calcite cultivated for 12 d had a higher crystalinity than that cultivated for 24. The result also illustrated that with the cultivation time Mg could damage the calcite crystal structure, which was well consistent with the conclusion deduced by the larger 2θ of calcite (104) with the cultivation time. FWHM of aragonite (111) at each kind of Mg/Ca molar ratio become smaller with the cultivation time, suggesting that the crystallinity of aragonite became better and the longer cultivation time were conducive to the increase of aragonite crystallinity in the presence of Mg^{2+} ions. The FWHM of aragonite (111) cultivated for 24 d also became smaller with the increasing of Mg/Ca molar ratio, revealing that the better crystallinity of aragonite was closely related to the higher concentration of Mg^{2+} ions, that is to say, Mg^{2+} ions have played an important role in the aragonite formation. In the control group, there was no mineral precipitates. The result also showed that *B. lichniformis* DB1-9 bacteria could release ammonia and bicarbonate and carbonate ions to increase the pH value and the supersaturation of the calcite and aragonite in the liquid culture medium and then the mineral precipitates could be harvested in the experimental group and then analyzed by different methods.

3.4 FTIR Analysis of the Minerals at Mg/Ca Molar Ratio of 3 Induced by B. lichniformis DB1-9 Bacteria.

The sample preparation work referenced Tian, B. et al; Wang, J. et al [81, 82]. The characteristic peaks of the minerals and organic functional groups can be obtained from Fig. 5. The characteristic peaks of calcite are 712, 875, 1421 and 2514 cm^{-1} and those of aragonite are at 710, 856, 1082 and

Preprints (www.preprints.org) | NOT PEER-REVIEWED | Posted: 12 October 2018 doi:10.20944/preprints201810.0267.v1

Peer-reviewed version available at Minerals 2018, 8, 585; doi:10.3390/min8120585

1475cm^{-1} [47, 48]. It can be seen from Fig. 5a that the peaks at 719, 877, and 2532 cm^{-1} are the characteristic peaks of calcite, and the peaks at 1083 and 1478 cm^{-1} prove the existence of aragonite, well consistent with the results of XRD analyses. Besides of the characteristic peaks of these

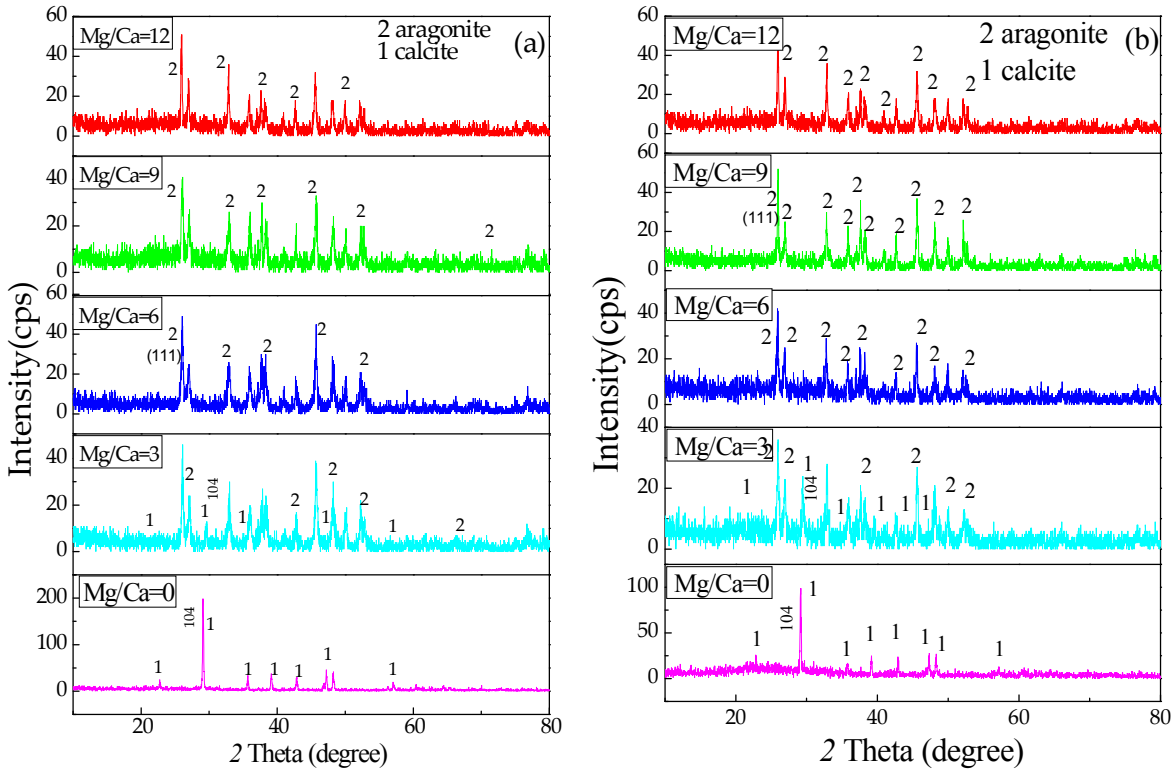

Figure 4. XRD analyses of the minerals induced by *B. lichniformis* DB1-9 bacteria. (a) the minerals cultivated for 12 d; (b) the minerals cultivated for 24 d.

minerals induced by *B. lichniformis* DB1-9 bacteria, there are also some peaks showing the other organic functional groups present in/on the minerals, such as C–H methylene vibrational band (2925 cm^{-1}), O-H vibrational band (2363 cm^{-1}), C=O vibrational band (1797 cm^{-1}), and C-O vibrational band (1077 cm^{-1}) shown in Fig. 5b and C=C, N-H, P=O, and C-O (glycosidic linkage) vibrational band at 1652, 1455, 1233, and 1084 cm^{-1} respectively shown in Fig. 5c, indicating that these organic functional groups of the metabolites secreted from *B. lichniformis* DB1-9 bacteria have a close releationship with the nucleation and growth of the minerals. As to which kind of specific organic functional group affects calcite and aragonite, further exploration is needed.

3.5 The Morphology and Elemental Composition of the Minerals Analyzed by SEM and EDX.

Fig. 6 shows the SEM and EDS results of the minerals after 24 days of cultivation. The calcites at Mg/Ca molar ratio of 0 show a elongation shape (Fig. 6a$_1$) and a dumbbell shape (Fig. 6a$_3$). The surface of the elongated calcite is covered with many small micron-sized rhombohedral calcites with a sharp corner, which were composed of a large amount of nano-meter mineral particles and were growing in a step mode (Fig. 6a$_2$). The dumbbell-shaped calcites grow symmetrically along the central axis and the surface is covered with many scale-like calcites (Fig. 6a$_4$), significantly different from the elongated calcite. At Mg/Ca molar ratio of 3, aragonite often exists in the form of aggregation(Fig. 6b$_1$) and the surface presents a large number of rectangular mineral growing parallelly(Fig. 6b$_2$). Some aragonite minerals show many holes in the surface (Fig. 6b$_3$), in which *B. lichniformis* DB1-9 bacteria lived. It can be seen from Fig. 6b$_4$ that there are EPS and microorganisms adsorbed on/among the mineral aggregates. These signigicant characteristics showed that the mineral formation was closely related to the activity of *B. lichniformis* DB1-9 bacteria. At Mg/Ca molar ratio of 6, some aragonite minerals are in a shape of cauliflower (Fig. 6c$_1$), and the surface of

Preprints (www.preprints.org) | NOT PEER-REVIEWED | Posted: 12 October 2018 doi:10.20944/preprints201810.0267.v1

Peer-reviewed version available at Minerals 2018, 8, 585; doi:10.3390/min8120585

cauliflower-shaped aragonite is covered with some holes and the granular minerals, no longer the rectangular minerals (Fig. 6c2). There are also some irregular aragonite aggregates (Fig. 6c3), whose suface are covered with a large number of flake-shaped minerals in a size of dozens of

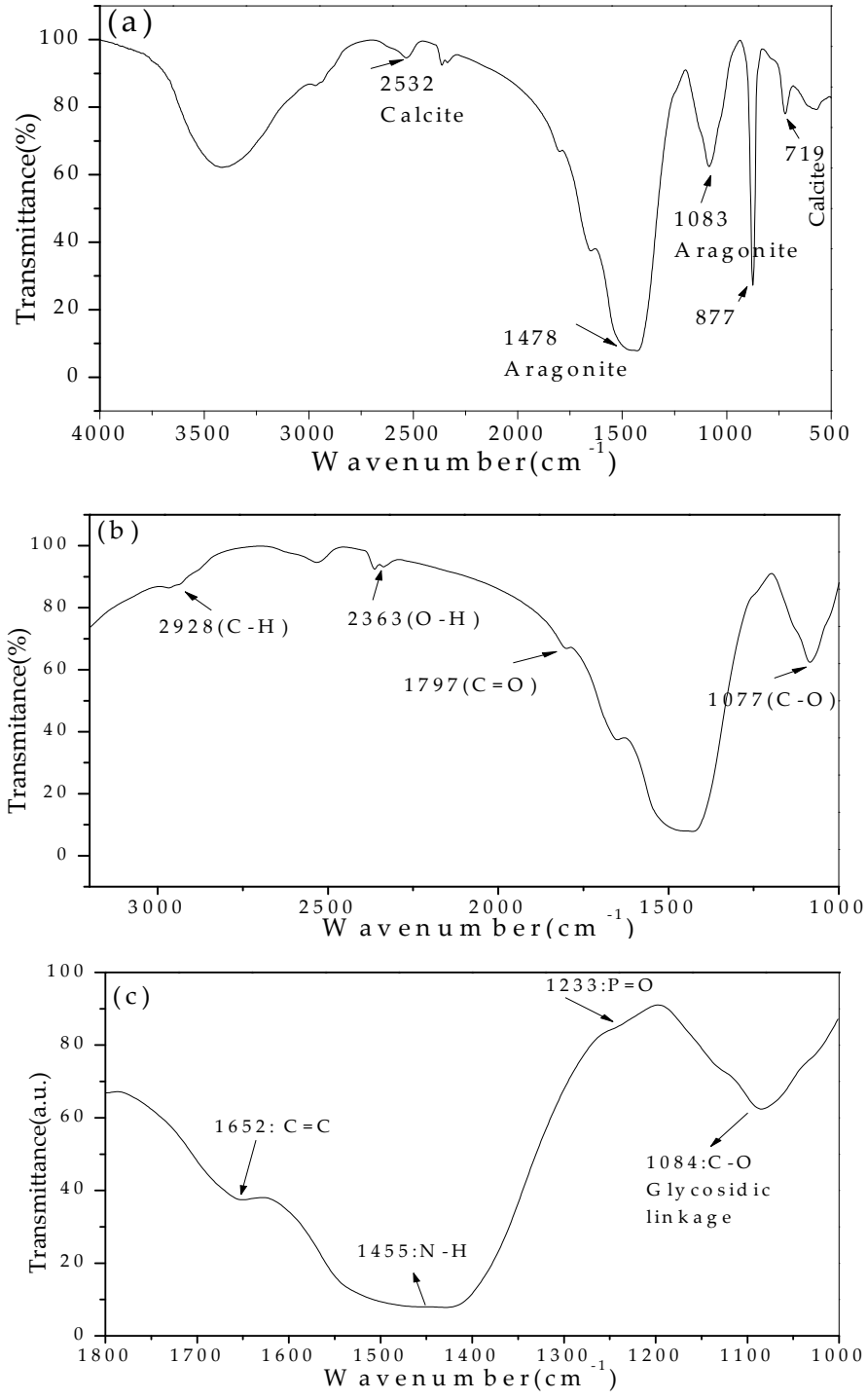

Figure 5. The minerals at Mg/Ca molar ratio of 3 analyzed by FITR.

a, the characteristics peaks of the minerals at Mg/Ca molar ratio of 3 from 500 - 4000 cm^{-1}; b, the FITR spectrogram of organic functional groups on/in the minerals at Mg/Ca molar ratio of 3 from 1000 - 3200 cm^{-1}; the FITR spectrogram of organic functional groups on/in the minerals at Mg/Ca molar ratio of 3 from 1000 - 1800 cm^{-1}.

nanometers (Fig. 6c4). Figs. 6 d1-d4 show the morphology of aragonite at Mg/Ca molar ratio of 9.

There are also irregular aragonite aggregates (Fig. 6d1), whose surface is also covered with flake-shaped minerals (Fig. 6d2) larger than those shown in Fig. 6c4. Besides this, there is spherical aragonite (Fig. 6d3) which is composed of a large amount of nano-meter granular minerals (Fig. 6d4). At Mg/Ca molar ratio of 12, aragonite presents a fusiform (Fig. 6e1) or fascicular (Figs. 6e2-e3) shape,

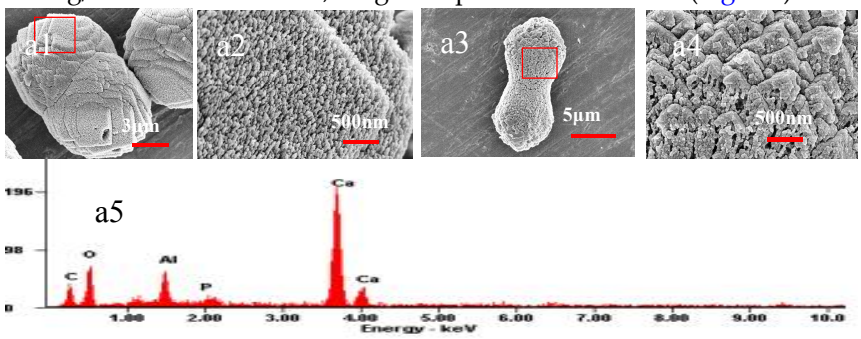

Mg/Ca=0

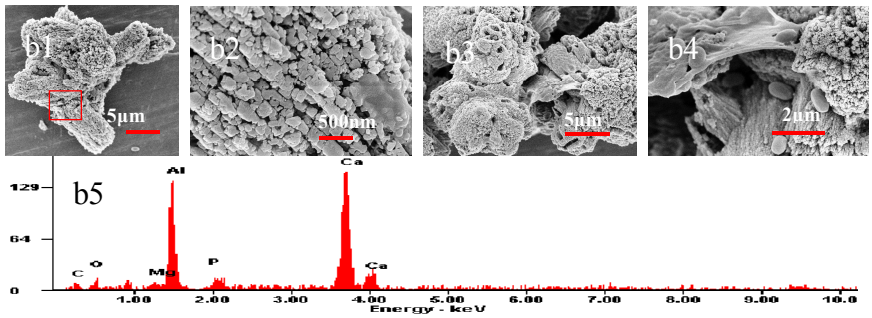

Mg/Ca=3

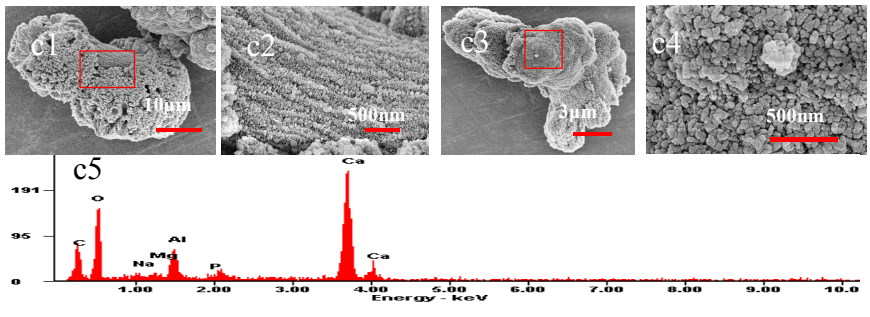

Mg/Ca=6

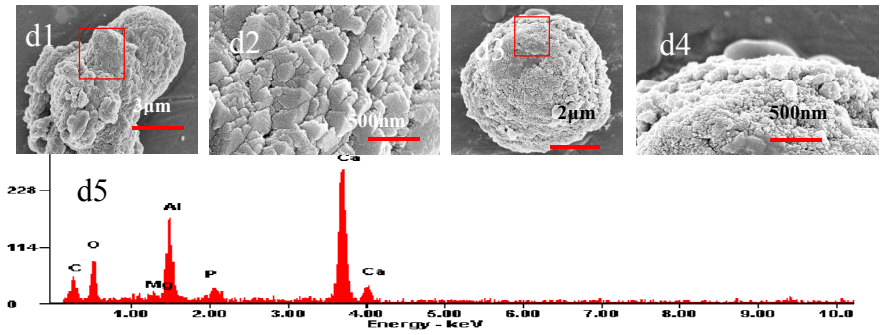

Mg/Ca=9

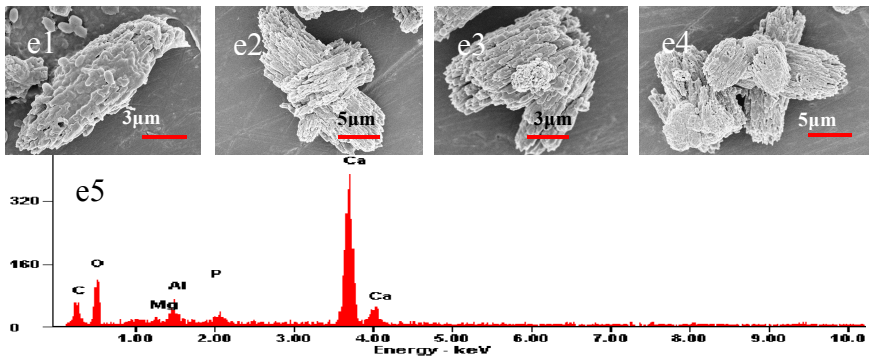

Mg/Ca=12

Figure 6. SEM and EDX images of minerals in the experimental groups after 24 days of cultivation. Mg/Ca molar ratio of 0 (a_1-a_4); Mg/Ca molar ratio of 3 (b_1-b_4); Mg/Ca molar ratio of 6 (c_1-c_4); Mg/Ca molar ratio of 9 (d_1-d_4); Mg/Ca molar ratio of 12 (e_1-e_4).

and also an aggregation state (Fig. 6e_4). EDS analyses show that there are Ca, C, O, Al and P elements in calcite at Mg/Ca molar ratio of 0 (Fig. 6a_5), besides of these elements, there is Mg elements in aragonite at other Mg/Ca molar ratios (Figs. 6b_5, c_5, d_5, e_5). P came from the metabolites or the *B. lichniformis* DB1-9 bacteria, and Mg came from $MgSO_4$ reagent in the culture medium.

3.6 Intracellular and Epicellular Biomineralization of B. lichniformis DB1-9 Bacteria analyzed by TEM.

The biomineralization induced by microorganisms includes three parts: the extracellular biomineralization, the intracellular biomineralization, and the epicellular biomineralization. The extracellular biomineralization aims to study the mineralogy, morphology and elemental composition, and funtional groups of the minerals induced by *B. lichniformis* DB1-9 bacteria. After finishing the above work, the next step is to study the intracellular biomineralization and the epicellular biomineralization. The ultrathin slices of *B. lichniformis* DB1-9 bacteria with a thickness of 70 nanometers have been prepared and analyzed by HRTEM-SAED. It can be seen from Fig. 7a_1 and a_2 that cell surface stratification is obvious, and there are different sizes of black areas inside the cells at Mg/Ca molar ratio of 0. Fig. 7a_3 and a_4 also show that there are larger dark granular areas in the space between the spore and the capsule, and there are dark granular areas in a size of dozens of nanometers adsorbed/grown on the EPS-like materials of the *B. lichniformis* DB1-9 bacteria. The formation of dark areas means that the density or thickness of the area is higher than other areas, which can block the penetration of electrons when analyzed by HRTEM. At Mg/Ca molar ratio of 3, there are also nano-meter granular areas dispersed inside the cell (Figs. 7b_1, b_2 and b_3) and adsorbed/grown on the EPS (Fig. 7b_4). At Mg/Ca molar ratio of 6, the dark area inside the cell become larger, gathering in the center of the cell marked by the red circle (Fig. 7c_1) or dispersing along the long axis of the cell marked by the red line (Fig. 7c_2). Near one end of the cell, there is larger blocky (Fig. 7c_3) or longer linear dark area (Fig. 7c_4) with a length of more than 100 nm, suggesting that the dark area becoming larger or longer maybe affected by the higher Mg^{2+} concentration. At Mg/Ca molar ratio of 9, there is a dark granular matter adsorbed in the inner membrane of the cell surface, with a length of more than 100 nm (Fig. 7d_1), and there are some dark matter dispersing inside the cell (Fig. 7d_2), and near the end of cell there is also existing the larger blocky (Fig. 7d_3) or longer linear dark area (Fig. 7d_4). At Mg/Ca molar ratio of 12, in addition to the above situation, another situation has arisen. Dark clumps composed of the alternating light and dark bands with a length of less than 100 nm appear on the EPS (Figs. 7e_1, e_3, and e_4; the detailes shown in Fig. 9), indicating that there were organic matter inside the dark clumps, that was to say, the organic matter maybe took part in or regulate the epicellular biomineralization. Many researchers have believed that the EPS can act as the nucleation site, and the idea has been accepted for many years. In this study, the formation of the dark clumps on the EPS has also proved this point. At the same time, if the intracellular dark nano-meter area could be as the site of biomineralization, we have also found that there are many nucleation sites besides of the EPS, such as the inner membranes of the surface and the membranes of the organells inside the cell. Therefore, the research results of intracellular mineralization and epicellular mineralization will enrich the previous conclusions.

In order to investigate the crystal structure of the dark granular or linear matter, SAED analyses were also performed. It can be obtained that there are a small number of diffraction spots in the SAED images (Figs. 8a_1, b_1, and c_1), indicating that the extracellular dark matters (Figs. 8a, b, and c) have a poor crystal structure. Intracellular dark matters (Figs. 8a_2, b_2, and c_2) have no crystal structures due to the fact that there are no diffraction spots in the SAED images (Figs. 8 a_3, b_3, and c_3). Many researchers have confused that why the amorphous matter still keep stable inside the cell. In general, the amorphous mineral is unstable and will turn into the stable mineral with better

crystal sturcture in the nature, such as ACC changing into calcite. The mechanism of keeping the amorphous matter stable inside the cell will be further explored in future. The dark clumps (Fig. 9a-c) composed of the alternating light and dark bands on the EPS of the cell were also further studied by SAED and the result shows that they still have no crystal structure (Fig. 9d). The question how such delicate structures are formed is also a mystery, and we are looking forward to solving the mystery in the future.

Although the intracellular and extracellular/epicellular dark granular or linear matter can be observed and the extracellular/epicellular dark matters have poor crystal structures and the intracellular linear and granular matters have no crystal structures, the elemental composition cannot still be known, thus, the next work is to investigate if the dark granular or linear matter contains Ca and Mg elements.

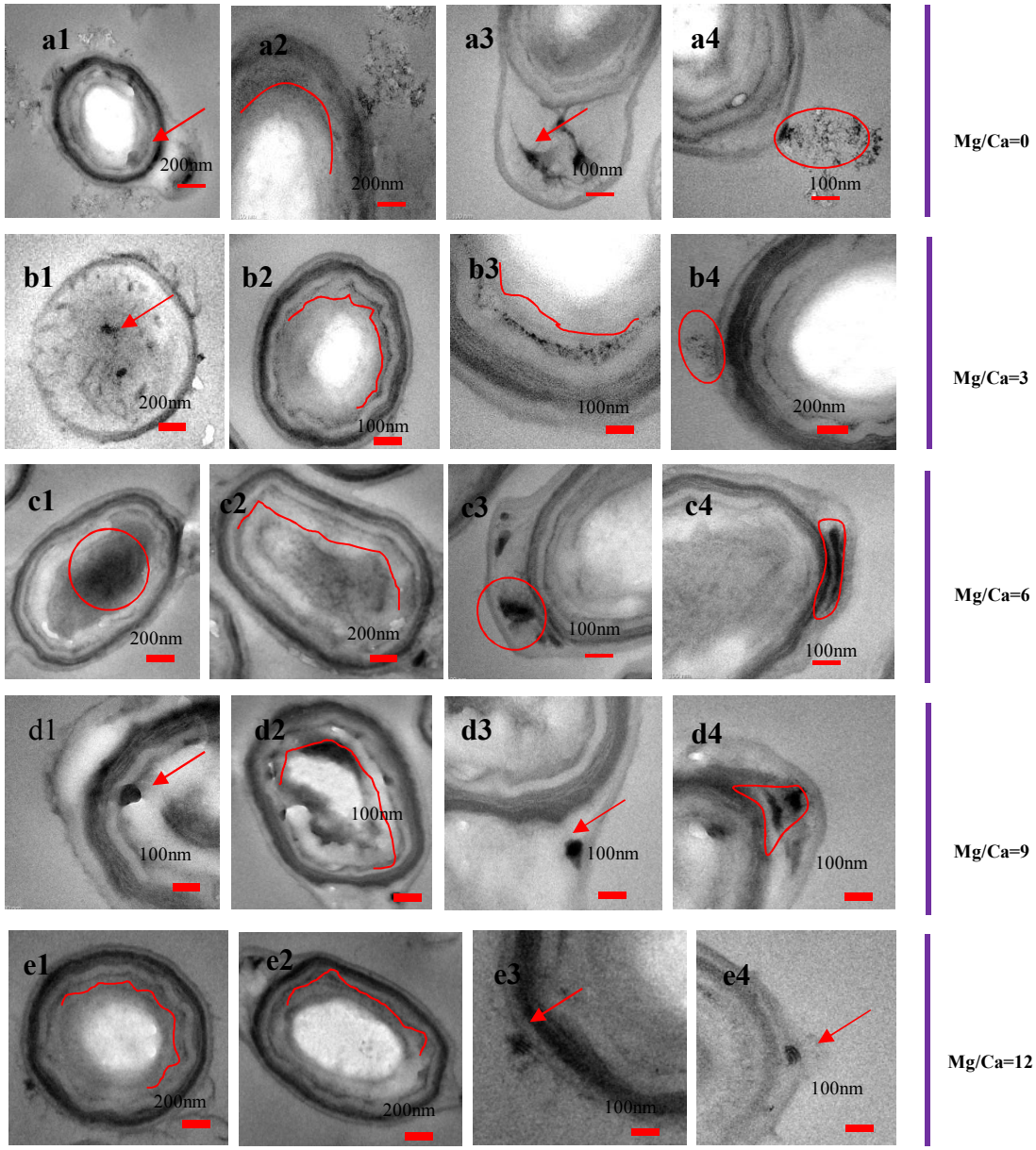

Figure 7. TEM analyses of the ultrathin slices of *B. lichniformis* DB1-9 bacteria cultivated for 24d. The intracellular and extracellular particels are marked with red arrows. Mg/Ca molar ratio of 0 (a_1-a_4): intracellular particles (a_1 and a_2) and extracellular particles (a_3 and a_4); Mg/Ca molar ratio of 3 (b_1-b_4): intracellular particles (b_1-b_3) and extracellular particles (b_4); Mg/Ca molar ratio of 6 (c_1-c_4): intracellular particles (c_1 and c_2) and extracellular particles (c_3 and c_4); Mg/Ca molar ratio of 9 (d_1-d_4): intracellular particles (d_1 and d_2) and extracellular particles (d_3 and d_4); Mg/Ca molar ratio of 12 (e_1-e_4): intracellular particles (e_1 and e_2) and extracellular particles (e_3 and e_4).

Peer-reviewed version available at Minerals 2018, 8, 585; doi:10.3390/min8120585

3.7 Ca and Mg Elemental Analysis of *B. lichniformis* DB1-9 Bacteria by STEM.

Fig. 10 show the morphology of *B. lichniformis* DB1-9 bacteria and the distribution of Ca and Mg elements. In the TEM images, the dark and denser areas inside the cell and on the cell EPS indicate the presence of metallic elements and the light area indicates the existence of organic matter in this study. However, in the STEM images, the result is reverse. Figs. 10 a, c, and e show that the surface of the cell is brightest, in a shape of light circle, the brightness decreases from outside to inside the cell, and the cell center is often the darkest area of the cell, suggesting that the concentration of metal element declined from outside to inside the cell. Fig. 10 b shows the distribution of Ca element in/on the *B. lichniformis* DB1-9 bacteria at Mg/Ca molar ratio of 0, also indicating that the concentration of Ca element was higher on the surface/EPS and inner membrane of the surface than that inside the cell.

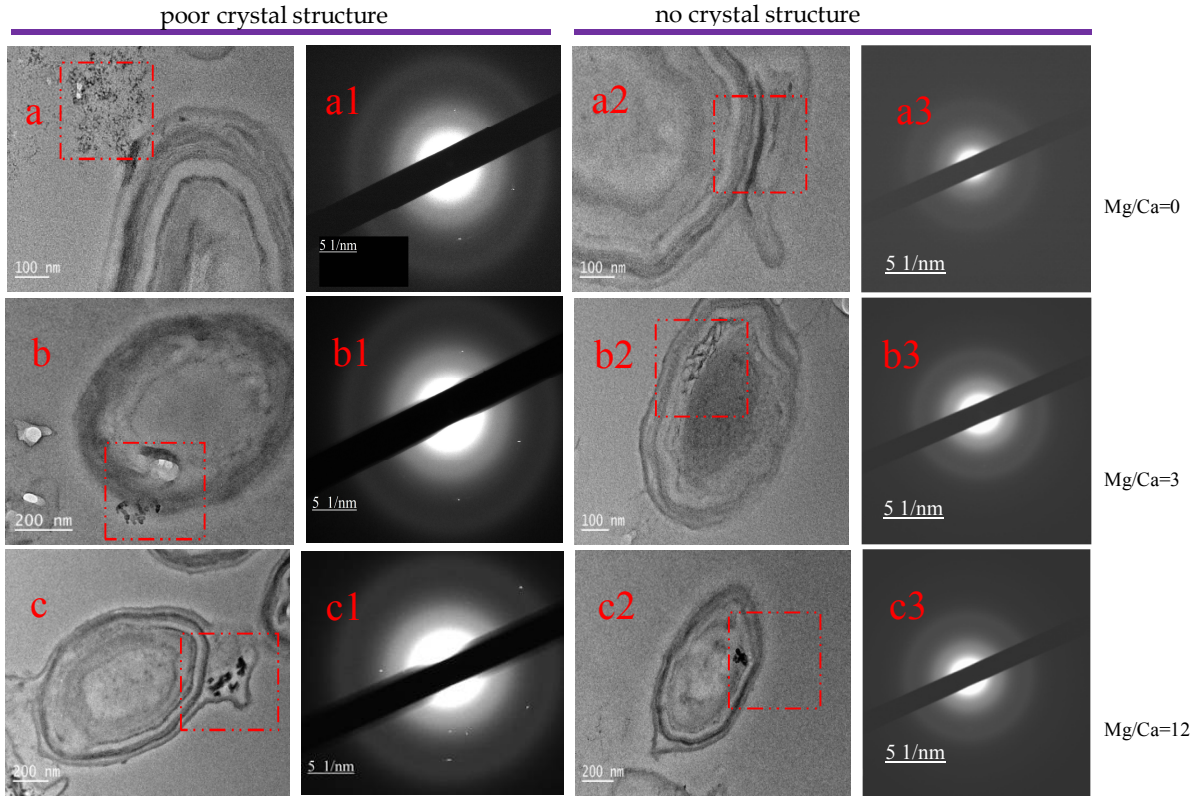

Figure 8. Analysis of intracellular and extracellular/epidermal dark matter by HRTEM-SAED. The HRTEM images of extracellular dark matter (a, b, and c), the SAED images of the area marked with the red square (a_1, b_1, and c_1). The HRTEM images of intracellular dark matter (a_2, b_2, and c_2), the SAED images of the area marked with the red square (a_3, b_3, and c_3). a_1, b_1, and c_1 show bright spots; a_3, b_3, and c_3 have no bright spots.

Figs. 10 c and d show the distribution of Ca and Mg elements in/on the *B. lichniformis* DB1-9 bacteria at Mg/Ca molar ratio of 3, also revealing the same rule that the concentrations of Ca and Mg decreased from outside the cell to inside the cell, that was to say, the transport mode of Ca^{2+} and Mg^{2+} ions was diffusion due to the fact that the metal ions were transferred along the concentration grade, namely from high to low concentration. Figs. 10 f and g show the distribution of Ca and Mg elements in/on the *B. lichniformis* DB1-9 bacteria at Mg/Ca molar ratio of 12. It can be observed that the concentration of Mg element is higher than that at Mg/Ca molar ratio of 3, suggesting that more and more Mg^{2+} ions could enter inside the cell by diffusion with the increase of Mg^{2+} ions concentration. These results also showed that the ability of *B. lichniformis* DB1-9 bacteria to prevent ions from entering the cell to protect themselves is limited. As we all know, Ca^{2+} and Mg^{2+} ions are cofactors of many enzymes in the cell, if without these ions, the enzymes will lose their activity, while if the concentrations of Ca^{2+} and Mg^{2+} ions are too high, they will have adverse effects on the

cell. In order to protect themselves, the only way was that a solid amorphous matter was formed by using the Ca^{2+} and Mg^{2+} ions transferred from the outside to inside the cell along the concentration grade. Thus, in my opinion, the amorphous dark granular and linear matter formed inside the cell and on the inner membrane of the cell surface maybe belonged to a protection mechanism.

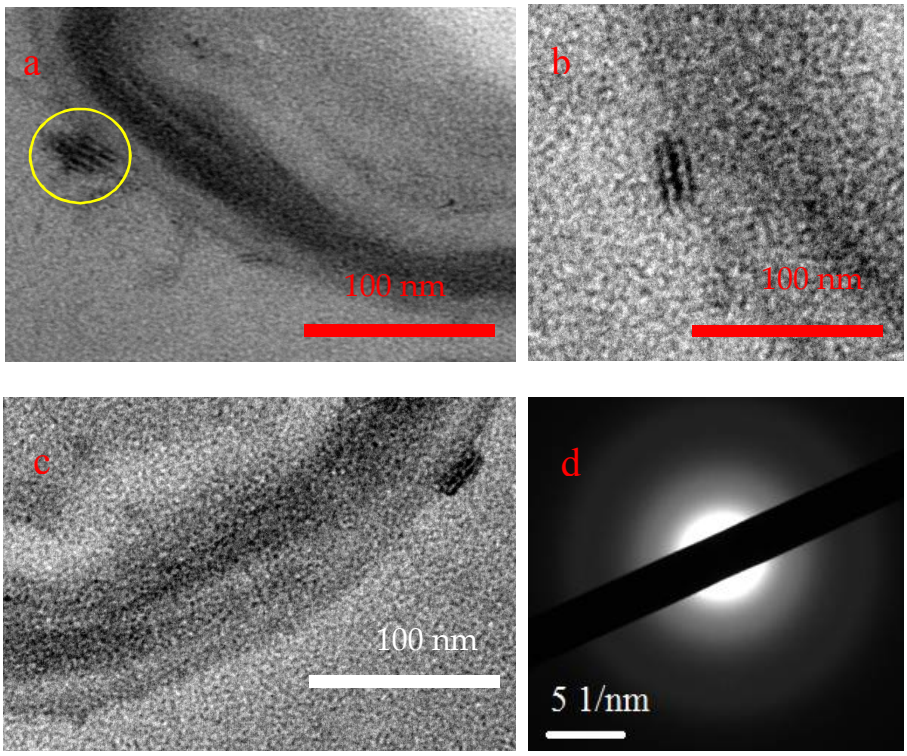

Figure 9. The dark clumps composed of the alternating light and dark bands on the outer surface of the *B. lichniformis* DB1-9 bacteria analyzed by HRTEM and SAED. a-c, the images of the dark clumps analyzed by HRTEM, d, SAED image of the dark clump marked by the yellow circle in Fig. 9a.

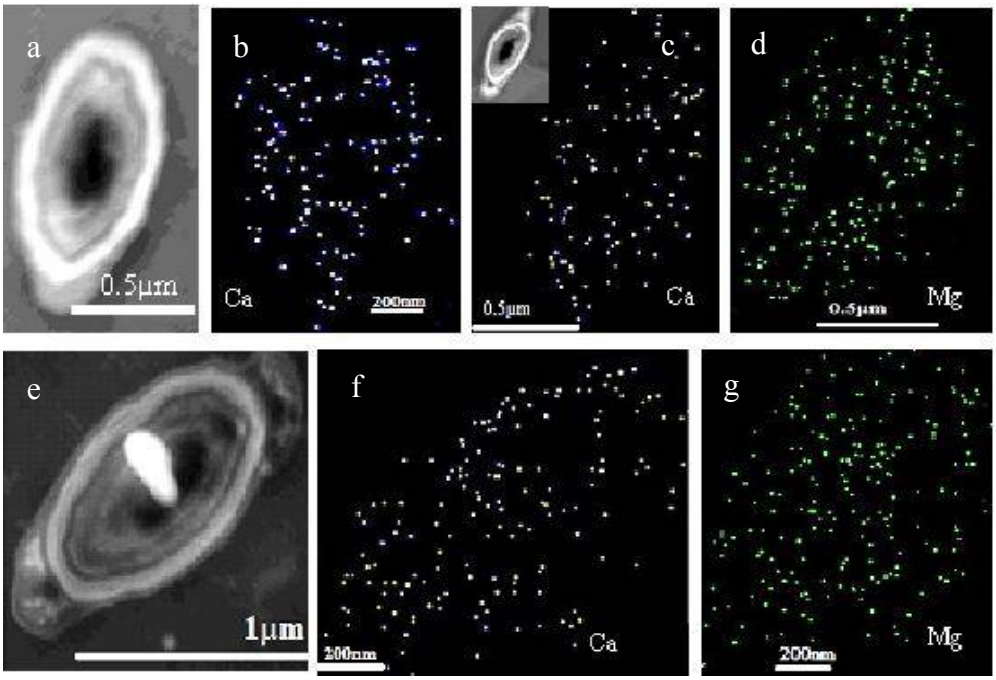

Figure 10. The morphology of *B. lichniformis* DB1-9 bacteria and elemental composition anayzed by STEM. a and b, Mg/Ca molar ratio of 0; c and d, Mg/Ca molar ratio of 3; e-g, Mg/Ca molar ratio of 12.

4. Discussion

Peer-reviewed version available at Minerals 2018, 8, 585; doi:10.3390/min8120585

4.1 The Mechanism of Extracellular Biomineralization Induce by B. lichniformis DB1-9 Bacteria

Microorganisms can increase the pH value and the alkalinity in the environment, which can reach the supersaturation to promote the mineral sedimentation. Many researchers have believed that the ammonia released from bacteria plays an important role in pH increase [83], however, there are many researchers who disagree with the opinion [41]. They have believed that the quantity of ammonia released from the bacteria is not enough to make pH increase so high, the pH values based on the ammonium concentration are much lower than those of the liquid culture medium inoculated with bacteria, besides of the ammonia, there should be other factor to affect pH increase, and finally CA is found to have the ability to make pH increase to such a high degree. Thus, both the ammonia and the CA were also investigated in this study.

The ammonia test showed that *B. lichniformis* DB1-9 bacteria could release the ammonia, revealing that pH value in the culture medium could be promoted according to the following equation (1):

$$NH_3 + H_2O \rightarrow NH_4^+ + OH^- \quad (1)$$

Besides of the ammonia, CA could also be secreted by *B. lichniformis* DB1-9 bacteria. So what does CA do? As we all know, cyanobacteria can increase pH in the liquid culture medium due to the fact that CA secreted by cyanobacteria can catalyze the hydration reaction of carbon dioxide to release the bicarbonate and carbonate ions when the photosynthesis of cyanobacteria happens [24]. With the increase of the concentration of bicarbonate and carbonate ions, pH in the liquid culture medium definitely increase. So it's always a headache that the high pH caused by cyanobacteria will result in the water pollution and the death of fish. The CA is a kind of metal enzyme widely present in microorganisms and plants [84-86], which includes acidic and alkaline CA [41]. In this study, pH could increase from 7.0 to 9.25, suggesting that the liquid culture medium was alkaline. There were still CA activities in such alkaline condition, indicating that CA secreted by *B. lichniformis* DB1-9 bacteria belonged to the alkaline CA. It has been reported that CA can be classified as one of the fastest reactive enzymes [87], if without CA catalysis, the hydration reaction of CO_2 is very slow [88], and the typical catalytic rate of different types of CA can be up to 10^4-10^6/s [87]. Thus, due to the existence of the alkaline CA in this study, the following equation (2) can occur:

$$CO_2 + H_2O \rightarrow H_2CO_3 \rightarrow HCO_3^- + H^+ \quad (2)$$

The ammonia dissolves into the water to produce a large number of hydroxyl groups (OH^-), which can react with H^+ to form water molecule, thus the equation (2) will go on to occur, at the same time, the following equation (3) will occur:

$$HCO_3^- + OH^- \rightarrow CO_3^{2-} + H_2O \quad (3)$$

Therefore, due to the existence of the ammonia, CA can release a large number of bicarbonate and carbonates ions, which can also increase the pH values in the culture medium. In this study, we can conclude that the pH increase is caused by the combination effect of the ammonia and the CA released by *B. lichniformis* DB1-9 bacteria, well consistent with the result of the reference by Zhuang et al., 2018.

It has been reported that CA produced by microbial metabolism plays an important role in biomineralization [29, 89]. The result of our study was well consistent with the above opinion. The existence of CA can produce enough quantity of bicarbonate and carbonate ions, and also make pH increase to 9.25 with the help of ammonia, therefore, the supersaturation of the carbonate minerals in the liquid culture medium can be elevated. Thus, the subsequent reaction can occur according to the following equation (4):

$$2Ca^{2+} + CO_3^{2-} + HCO_3^- + OH^- \rightarrow CaCO_3\downarrow + H_2O \quad (4)$$

If there is no CA production and alkaline environment, the minerals will not be produced in this study, which was confirmed by the absence of mineral formation in the control group. Therefore, microorganism, *B. lichniformis* DB1-9 bacterium, plays an important role in the biomineralization of carbonate mineral in this study. We can say that there is no formation of carbonate minerals if without microorganism.

Peer-reviewed version available at Minerals 2018, 8, 585; doi:10.3390/min8120585

4.2 The Relationship Between Organic Functional Groups and the Morphology of the Minerals and the Epicellular and Intracellular Biomineralization

In this study, many different kinds of organic functional groups (Figs. 5b and 5c) have been found, such as C-H, O-H, C=O, C-O, C=C, N-H, P=O etc. No matter these organic functional groups come from what kind of organic substance, no matter whether they are adsorbed on the surface of the mineral or exist inside the mineral, these organic functional groups are closely related to the mineral. Many researchers have believed that the morpholgy of the minerals can be affected by the organic functional groups [90-95]. The elongated calcite could be obtained in this study and its morphology maybe was related to C=O group, which maybe came from polysacharides, simple sugars, or organic matter containing carboxyl groups. Oxygen atom in C=O group carries negative charges, which means that it can interact with the polar surface of the minerals and cannot affect the neutral surface. Through the influence of organic functional groups, the growth rate of some crystal planes of mineral crystals will change, thus changing the morphology of mineral crystals. It has been reported that the biological macromolecules containing abundant carboxyl groups tend to interact with the stronger polar crystal plane of calcite, whereas the other macromolecules with less acidity interact with the neutral crystal plane, thus beneficial to the formation of elongated calcite [90-92]. There are many studies like this, for example, the proteins coming from sea-urchin and mollusc shells are always glycosylated and contains the glycosidic groups (-C-O-C-), which can help to form the unique morphology of minerals [28, 91-97].

B. lichniformis DB1-9 bacterium belongs to Gram-positive bacteria, which means that the surface and EPS of the *B. lichniformis* DB1-9 bacterium contains a large quantity of peptidoglycan. From the result of FTIR, N-H group can be found, which was maybe coming from the peptidoglycan of the cell EPS. Nitrogen atoms from the N-H groups also carry negative charges and also adsorb a large number of Ca^{2+} and Mg^{2+} ions, thus forming a dense ring of Ca^{2+} and Mg^{2+} ions around the cell surface, which was well consistent with the result of STEM analyses (Figs. 10b-10d and 10f and 10g). The minerals growing on the cell EPS had a poor crystalinity (Figs. $8a_1$ and $8b_1$ and $8c_1$), on the contrary, calcite with better crystalinity can grow arround the cell surface of cyanobacteria *Synechocystis* sp. PCC6803 [27], which was maybe due to the different species of bacteria or maybe due to the damage of calcite by Mg^{2+} ions. Many scholars have found that EPS is a momentous material in the biomineralization process [18, 29, 39, 47, 97-100]. The STEM result revealed that our conclusion was well consistent with the above opinions. The organic functional groups on the cell EPS can not only reduce the nucleation energy and make the whole process of biomineralization to be more easily [101] but also promote the nucleation [102].

P=O group can also be found in FTIR result, which maybe came from the phospholipids in the cell membranes or deoxyribonucleic acid (DNA) or ribonucleic acid (RNA). The negative charged oxygen atoms in the P=O groups, which were loacted in the phospholipids of the cell membranes, can also adsorb Ca^{2+} and Mg^{2+} ions, thus leading to the nano-meter dark matters growing on the inner membrane inside the cell surface (Figs. 7d1 and 7d2 and 7d4). Maybe the intracellular organic functional groups were helpful to form the amorphous nano-meter matters inside the cell, which was not only beneficial to the intracellular biomineralization but also helpful to protect themselves. Although the metal ions do not easily enter the cell, the Ca^{2+} can enter the cell through the ion channel [103]. Besides of the intracellular biomineralizaiont, the EDS (Fig. 6) result also shows that the P element appears in the calcite and aragonite, which maybe derived from the bacteria. The EDS result was well consistent with that of FTIR. The P in minerals is one of the important evidences of the biomineralization induced by bacterium in the culture medium without P element [25].

It has been reported that the ingredients and structures of minerals can be change by bacteria [96, 104, 105], that is to say, the bacteria can not only change the composition of minerals but also control the morphology of minerals [47, 96, 105]. Therefore, *B. lichniformis* DB1-9 bacteria could lead to the preferential growth of some crystal planes of minerals and thus modify the mineral morphology by using many different kinds of organic functional groups.

4.3 the Relationship Between the Mg/Ca Molar Ratio and Calcium Carbonate Minerals

Peer-reviewed version available at Minerals 2018, 8, 585; doi:10.3390/min8120585

Many researchers have investigated the fluid inclusions derived from the ancient primary marine halite and drawn a conclusion that the Mg/Ca ratio of seawater has changed in a range of 1.0-5.2 throughout the Phanerozoic Eon [106-108]. The transition of the polymorph mineralogy of calcium carbonate precipitates throughout Phanerozoic time was caused by the variations of Mg/Ca ratios, which has been accepted for many years. When low seawater Mg/Ca<2 present, the predominant calcium carbonate was calcite or low Mg calcite (i.e., calcite seas); when high seawater Mg/Ca>2 present, high Mg calcite and aragonite became the predominant polymorphs of calcium carbonate (i.e., aragonite seas) [109]. In this study, Mg/Ca molar ratios have been set as 0, 3, 6, 9, and 12 and the result also shows that aragonite was the only mineral phase when Mg/Ca molar ratio beyond 3 and calcite was the predominant mineral at Mg/Ca molar ratio of 0 and 3, also indicating that Mg/Ca molar ratios have played an important role in the formation of polymorphs of calcium carbonate. However, there were no minerals formed in the control groups, which had the same Mg/Ca molar ratios as the experimental group. Why? Thus, there were still other factors to influence the formation of calcite seas or aragonite seas besides of Mg/Ca molar ratios. In my opinion, microorganisms have played significant role in the transtition of calcite seas to aragonite seas. The only difference bwteen the control goup and the experimental group was the existence of *B. lichniformis* DB1-9 bacteria. There were no minerals in the control group, mainly due to the fact that the control groups were not inoculated with *B. lichniformis* DB1-9 bacteria. Although the different Mg/Ca molar ratios have been set in the control groups, there were still no minerals formed if without *B. lichniformis* DB1-9 bacteria, suggesting that biological factors could not be neglected during the transition process of calcite seas to aragonite seas. *Ries et al.* have conducted the experiments to investigate the important role played by the varied seawater Mg/Ca molar ratio on biomineralization within marine bacterial biofilms, and found that the biomineralization occurred exclusively on the biofilm plates and none on the non-biofilm control plates [110]. Therefore, as for the reason of the transition of calcite seas to aragonite seas, biological factors should be considered besides of the pCO_2, Mg/Ca molar ratios, salinities, temperatures etc.

In this study, Ca^{2+} ions have taken part in the formation of calcite and aragonite, however, Mg^{2+} ions have been neglected. In my opinion, Mg^{2+} ions should be involved into the formation of magnesium carbonate or magnesium phosphate just like Ca^{2+} ions in the liquid culture medium. However, the result was converse to my guess. Mg^{2+} ions always exist as ions, and no magnesium mineral is formed. Maybe Mg^{2+} ions need longer time than Ca^{2+} ions to form the magnesium carbonate or magnesium phosphate. It has been reported that the most difficult step is the dehydration of hydrated cations in the formation of cation-carbonate pairs [28]. The enthalpy of $Mg[H_2O]_6^{2+}$ dehydration is 351.8 kal/mol, and that of $Ca[H_2O]_6^{2+}$ is 264.3 kal/mol at room temperature and natural pression (298K, 1 atm) [28]. It may be that the presence of hydrated membranes makes it difficult for Mg^{2+} ions to form mineral crystals. But some researchers have other different opinions. For example, *Xu et al., 2013* have conducted the experiments and believed that Mg^{2+} ions in dry formamide can still not take part in the formation of magnesium carbonate crystals [111]. The Mg^{2+} ions without hydrated membrane should react with CO_3^{2-} ions quickly due to the fact that energy is not needed to remove the water molecules around the Mg^{2+} ions. Finally *Xu et al., 2013* have found that the lattice limitation on the spatial configuration of CO_3^{2-} groups, other than cation hydration, prevents Mg^{2+} and CO_3^{2-} ions from forming long-range ordered structures [111]. The mechanism of Mg^{2+} biomineralization induce by microorganism should be further explored in future.

4.4 the Transport Mode of Ca^{2+} and Mg^{2+} Ions and the Nucleation Site

There were a large number of Ca^{2+} and Mg^{2+} ions adsorbed on/in the suface/EPS shown in Fig. 10, besides of this, Ca^{2+} and Mg^{2+} ions could also enter the cell (Fig. 10), indicating that the transport mode of Ca^{2+} and Mg^{2+} ions belonged to the diffusion because these ions were transferred from the outside to inside the cell and along a concentration grade from a high to low concentration. As we all know, the soluble ions cannot easily enter the cell due to the barrier of cell membrane, which is composed of phospholipid bilayer and can prevent the Ca^{2+} and Mg^{2+} ions from entering the cell.

However, there are Ca^{2+} channels located in the cell membrane, which can act as the carriers to transfer Ca^{2+} ions from the outside to inside the cell. It has been reported that the voltage-gated Ca^{2+} channel can mediate Ca^{2+} entry into cells in response to membrane depolarization [112] and the membrane-embedded ion channels are electrolyte-filled nanotubes with different kinds of proteins [113]. Such a transport through Ca^{2+} channels is called facilitated diffusion, which is much faster than the simple diffusion that there are no carriers. Similarly, we have also believed that there are Mg^{2+} channels in addition to Ca^{2+} channels. Some researchers have reported that the primary uptake system, namely the CorA Mg^{2+} channel, is present in about half of all bacteria and archaea [114]. Therefore, Mg^{2+} ions could also be transferred through the Mg^{2+} channels by diffusion. When Ca^{2+} and Mg^{2+} ions are present outside the cell at the same time, the factors governing the selectivity filter of voltage-gated Ca^{2+} ion channel lie in the pore size, oligomericity, and solvent accessibility [115]. That is to say, Mg^{2+} ions can also enter the cell through Ca^{2+} ion channel by diffusion. Thus, many Ca^{2+} and Mg^{2+} ions can be observed inside the cell and on/in the surface/EPS shown in Fig. 10.

As for the nucleation site, many researchers have believed that the microbial cell surface and EPS have played important roles [116-119]. However, some researchers have different opinions and have found from their conducted experiment that the dolomite minerals can not be observed on the heat-killed cell surface [31], which means that the cell surface alone is not sufficient to serve as the nucleation site. In my opinion, there are many amino acids in/on the surface of cells, such as glutamic acid and aspartic acid in some kind of Ca^{2+} channel, which can bind mental ions like Ca^{2+} and Mg^{2+} ions. If the bacteria cells were heat-killed at a enough high temperature, these amino acids in/on the surface of cells may be destroyed and missing, which was not beneficial to the adsorbtion of metal ions. That is to say, we have agreed the opinion that the cell surface alone is not sufficient to serve as the nucleation site. There should be other factors which are present in the surface of cells to affect the adsorbtion and nucleation of the metal ions. Besides of the cell surfaces, the EPS around the cell surface may have also played an important role [35, 36, 119]. In the experiments performed by *deng et al.* the sulfate-reducing bacteria (SRB) and halophilic bacteria have EPS-like materials, which may have served as the nucleation site for dolomite [31]. In our research, there are also EPS-like materials around the cell surface, in which there are also nano-meter matters with poor crystalinity. Thus, the EPS of bacteria were also as the nucleation sites. However, if the EPS were isolated from the cell surface by heat method and used to induce the minerals, the question whether the nucleation site was still on/in the heated EPS needs further study.

5. Conclusion

In this study, *B. lichniformis* DB1-9 bacteria were identified by 16S rDNA sequences and used to induce carbonate minerals at different Mg/Ca molar ratios. The pH values can increase to 9.25 mainly due to the combination effect of CA and ammonia released by *B. lichniformis* DB1-9 bacteria. CA can catalyze the hydration reaction of carbon dioxide to release a large number of bicarbonate and carbonate ions, which can elevate the supersaturation of the calcium carbonate in the liquid culture medium and promote the precipitation of polymorphs of calcium carbonate. The existence of Mg^{2+} ions and some kinds of organic functional groups can affect the morphology of minerals. The formation of aragonite mineral is not only related to Mg^{2+} ions but also has a strong correlation with the presence of microorganisms. The formed intracellular nano-meter matter has no crystal structure, and while the nano-meter particle on/in the EPS of the cell has a poor crystal strucure. This study maybe can help to understand the transition process and mechanism of calcite seas to aragonite seas, and also help to further understand the biomineralization mechanism induced by microorganisms.

Acknowledgments: This work was supported by the National Natural Science Foundation of China (41772095, U1663201, 41702131), Taishan Scholar Talent Team Support Plan for Advanced & Unique Discipline Areas, Major Scientific and Technological Innovation Projects of Shandong Province (2017CXGC1602, 2017CXGC1603), SDUST Research Fund (2015TDJH101), Natural Science Foundation of Shandong Province (ZR2017BD001), the China Postdoctoral Science Foundation founded project (2016M600548, 2017T100502), Qingdao Postdoctoral Applied Research Project (2015199), the Scientific and Technological Innovation Project

Financially Supported by Qingdao National Laboratory for Marine Science and Technology (No. 2016ASKJ13), Open Fund of the Key Laboratory of Marine Geology and Environment, Chinese Academy of Sciences (No. MGE2016KG10).

Author Contributions: Zuozhen Han conceived and designed the experiments; Xiao Gao performed the experiments; Zuozhen Han, Hui Zhao, and Huaxiao Yan analyzed the results of all the experiments; Xiao Gao and Huaxiao Yan wrote the paper. Hui Zhao revised the manuscript. All authors read and approved the manuscript.

Conflicts of Interest: The authors declare no conflict of interest.

References

1. Lee, J.H.; Chen, J.; Choh, S.J. Furongian (Late Cambrian) sponge–microbial maze-like reefs in the North China Platform. Palaios, 2014, 29, 27-37. DOI: 10.2110/palo.2013.050
2. Yang, R.C.; Fan, A.P.; Han, Z.Z. Characteristics and genesis of microbial lumps in the Maozhuang Stage (Cambrian Series 2), Shandong Province, China. *Science China Earth Sciences*, **2013**, 56, 494-503. DOI: 10.1007/s11430-012-4539-4
3. Chang, X.; Shi, B.; Han, Z.; Li, T. C_5-C_{13}, light hydrocarbons of crude oils from northern Halahatang oilfield (TarimBasin, NW China) characterized by comprehensive two-dimensional gas chromatography. *Journal of Petroleum Science and Engineering*. **2017**, 157, 223-231 DOI: 10.1016/j.petrol.2017.07.043
4. Liu, J.; Yao, Y.; Elsworth, D. Vertical Heterogeneity of the Shale Reservoir in the Lower Silurian Longmaxi Formation: Analogy between the Southeastern and Northeastern Sichuan Basin, SW China. *Minerals*, **2017**, 7, 1-17, DOI: 10.3390/min7080151
5. Wang, G.; Chang, X.; Yin, W. Impact of diagenesis on reservoir quality and heterogeneity of the Upper Triassic Chang 8 tight oil sandstones in the Zhenjing area, Ordos Basin, China. *Marine and Petroleum Geology*, **2017**, 84-96. Doi:10.1016/j.marpetgeo.2017.03.008
6. Han, C.; Jiang, Z.; Han, M. The lithofacies and reservoir characteristics of the Upper Ordovician and Lower Silurian black shale in the Southern Sichuan Basin and its periphery, China. *Marine and Petroleum Geology*, **2016**, 75,181-191. DOI:10.1016/j.marpetgeo.2016.04.014
7. Liu, X.H.; Luo, J.L. Diagenesis and diagenetic facies of gas reservoirs in the Upper Paleozoic 8th member of Shihezi Fm and 2nd member of Shanxi Fm in Yulin-Shenmu area, Ordos basin. *Oil and Gas Geology*, **2006**, 2, 010.
8. Chen, J.T.; Chough, S.K.; Chun, S.S. Limestone pseudoconglomerates in the Late Cambrian Gushan and Chaomidian Formations (Shandong Province, China): soft-sediment deformation induced by storm-wave loading. *Sedimentology*, **2009**, 56(4): 1174-1195. DOI: 10.1111/j.1365-3091.2008.01028.x
9. Chen, J.T.; Chough, S.K.; Han, Z.; Lee, J.H. An extensive erosion surface of a strongly deformed limestone bed in theGushan and Chaomidian formations (late middle Cambrian to Furongian), Shandong Province, China: sequence-stratigraphic implications. *Sedimentary Geology*, **2011**, 233, 129-149. DOI: 10.1016/j.sedgeo.2010.11.002
10. Chen, J.T.; Chough, S.K.; Lee, J.H.; Han, Z.; Sequence-stratigraphic comparison of the upper Cambrian series 3 toFurongian succession between the Shandong region, China and the Taebaek area, Korea: high variability of bounding surfaces in an Epeiric platform. *Journal of Geosciences*, **2012**, 16, 357-379. DOI: 10.1007/s12303-012-0040-5

11. Chen, J.T.; Han, Z.Z.; Zhang, X.L.; Fan, A.P.; Yang, R.C. Early diagenetic deformation structures of the Furongianribbon rocks in Shandong Province of China-A new perspective of the genesis of limestone conglomerates. *Science China. Earth Sciences*, **2010**, 53, 241-252.DOI: 10.1007/s11430-010-0010-6
12. Chen, J.T.; VanLoon, A.J.; Han, Z.; Chough, S.K. Funnel-shaped, breccia-filled clastic dykes in the late Cambrian Chaomidian formation (Shandong Province, China). *Sedimentary Geology*, **2009**, 221, 1-6. DOI: 10.1016/j.sedgeo.2009.09.006
13. Han, Z.; Zhang, X.; Chi, N.; Han, M.; Woo, J.; Lee, H.S. Cambrian oncoids and other microbial-related grains on thenorth china platform. *Carbonate Evaporite,* **2015**, 30, 373-386. DOI: 10.1007/s13146-014-0209-2
14. Planavsky, N.; Reid, R.P.; Lyons, T.W. Formation and diagenesis of modern marine calcified cyanobacteria. *Geobiology*, **2010**, 7, 566-576, DOI: 10.1111/j.1472-4669.2009.00216.x
15. Cam, N.; Georgelin, T.; Jaber, M. In vitro synthesis of amorphous Mg-, Ca-, Sr-and Ba-carbonates: what do we learn about intracellular calcification by cyanobacteria? *Geochimica et Cosmochimica Acta*, **2015**, 161, 36-49. DOI: 10.1016/j.gca.2015.04.003
16. Bundeleva, IA.; Menez, B.; Augé, T. Effect of cyanobacteria Synechococcus PCC 7942 on carbonation kinetics of olivine at 20° C. *Minerals Engineering*, **2014**, 59, 2-11. DOI: 10.1016/j.mineng.2014.01.019
17. Bundeleva, IA.; Shirokova, L.S.; Pokrovsky, O.S. Experimental modeling of calcium carbonate precipitation by cyanobacterium Gloeocapsa sp. *Chemical Geology*, **2014**, 374, 44-60. DOI: 10.1016/j.chemgeo.2014.03.007
18. Obst, M.; Dynes, J.J.; Lawrence, J.R. Precipitation of amorphous $CaCO_3$, (aragonite-like) by cyanobacteria: A STXM study of the influence of EPS on the nucleation process. *Geochimica et Cosmochimica Acta*, **2009**, 73, 4180-4198, DOI: 10.1016/j.gca.2009.04.013.
19. Martinez, R.E.; Gardés, E.; Pokrovsky, O.S. Do photosynthetic bacteria have a protective mechanism against carbonate precipitation at their surfaces?. *Geochimica et Cosmochimica Acta*, **2010**, 74, 1329-1337. DOI: 10.1016/j.gca.2009.11.025
20. Power, I.M.; Wilson, S.A.; Thom, J.M. Biologically induced mineralization of dypingite by cyanobacteria from an alkaline wetland near Atlin, British Columbia, Canada. *Geochemical Transactions*, **2007**, 8, 13.
21. Kempe, S.; Kazmierczak, J. Calcium carbonate supersaturation and the formation of in situ calcified stromatolites. *Facets of modern biogeochemistry*, **1990**, 255-278.
22. Han, Z.; Yan, H.; Zhou, S. Precipitation of calcite induced by Synechocystis sp. PCC6803. *World Journal of Microbiology and Biotechnology*, **2013**, 29, 1801-1811.
23. Han, Z.; Yan, H.; Zhao, H. Bio-precipitation of calcite with preferential orientation induced by Synechocystis sp. PCC6803. *Geomicrobiology Journal*, **2014**, 31, 884-899.
24. Han, Z.; Meng, R.; Yan, H. Calcium carbonate precipitation by Synechocystis sp. PCC6803 at different Mg/Ca molar ratios under the laboratory condition. *Carbonates and Evaporites*, **2017**, 32, 561-575.
25. Han, Z.; Zhao, Y.; Yan, H. The Characterization of Intracellular and Extracellular Biomineralization Induced by Synechocystis sp. PCC6803 Cultured under Low Mg/Ca Ratios Conditions. *Geomicrobiology*, **2017**, 34, 362-373, DOI: 10.1080/01490451.2016.1197986.

26. Han, Z.; Zhuang, D.; Yan, H. Thermogravimetric and kinetic analysis of thermal decomposition characteristics of microbial calcites induced by cyanobacteria Synechocystis sp. PCC6803. *Journal of Thermal Analysis and Calorimetry*, **2017**, 127, 1371-1379. DOI: 10.1007/s10973-016-6026-1
27. Yan, H.; Han, Z.; Zhao, H. Characterization of calcium deposition induced by Synechocystis sp. PCC6803 in BG11 culture medium. *Chinese journal of oceanology and limnology*, **2014**, 32, 503-510. DOI: 10.1007/s00343-014-3150-2
28. Qiu, X.; Wang, H.; Yao, Y. High salinity facilitates dolomite precipitation mediated by Haloferax volcanii DS52. *Earth & Planetary Science Letters*, **2017**, 472, 197-205.
29. Han, Z.; Li, D.; Zhao, H.; Yan, H.; Li, P. Precipitation of Carbonate Minerals Induced by the Halophilic Chromohalobacter Israelensisunder High Salt Concentrations: Implications for Natural Environments. *Minerals*, **2017**, 7, 1-27, DOI: 10.3390/min7060095.
30. Rivadeneyra, M.; Párraga, J.; Delgado, R. Biomineralization of carbonates by Halobacillus trueperi in solid and liquid media with different salinities. *FEMS Microbiology Ecology*, **2004**, 48, 39-46. DOI: 10.1016/j.femsec.2003.12.008
31. Deng, S.; Dong, H.; Lv, G. Microbial dolomite precipitation using sulfate reducing and halophilic bacteria: Results from Qinghai Lake Tibetan Plateau NW China. *ChemicalGeology*, **2010**, 278, 151-159. DOI: 10.1016/j.chemgeo.2010.09.008
32. Han, Z.; Zhao, Y.; Yan, H. Struvite Precipitation Induced by a Novel Sulfate-Reducing Bacterium Acinetobacter calcoaceticus SRB4 Isolated from River Sediment. *Geomicrobiology Journal*, **2015**, 32, 868-877. DOI: 10.1080/01490451.2015.1016247
33. Braissant, O.; Decho, A.W.; Dupraz, C. Exopolymeric substances of sulfate-reducing bacteria: interactions with calcium at alkaline pH and implication for formation of carbonate minerals. *Geobiology*, **2007**, 5, 401-411. DOI: 10.1111/j.1472-4669.2007.00117.x
34. Bontognali, T.R.R.; McKenzie, J.A.; Warthmann, R.J. Microbially influenced formation of Mg-calcite and Ca-dolomite in the presence of exopolymeric substances produced by sulphate-reducing bacteria. *Terra Nova*, **2014**, 26, 72-77. DOI: 10.1111/ter.12072
35. Kenward, P.A.; Goldstein, R.H.; Gonzalez, L.A. Precipitation of low-temperature dolomite from an anaerobic microbial consortium: the role of methanogenic Archaea. *Geobiology*, **2009**, 7, 556-565. DOI: 10.1111/j.1472-4669.2009.00210.x
36. Sánchez-Román, M.; Vasconcelos, C.; Warthmann, R. Microbial dolomite precipitation under aerobic conditions: results from Brejo do Espinho Lagoon (Brazil) and culture experiments. Perspectives in Carbonate Geology: A Tribute to the Career of Robert Nathan Ginsburg, **2009**, 41: 167-178.
37. Lv, J.J.; Ma, F.; Li, F.C. Vaterite induced by Lysinibacillus sp. GW-2 strain and its stability. *Journal of structural biology*, **2017**, 200, 97-105. DOI: 10.1016/j.jsb.2017.09.008
38. González-Muñoz, M. T.; Rodriguez-Navarro, C.; Martínez-Ruiz, F. Bacterial biomineralization: new insights from Myxococcus-induced mineral precipitation. *Geological Society, London, Special Publications*, **2010**, 336, 31-50. DOI: 10.1144/SP336.3
39. Rodriguez-Navarro, C; Jimenez-Lopez, C.; Rodriguez-Navarro, A. Bacterially mediated mineralization of vaterite. *Geochimica Et Cosmochimica Acta*, **2007**, 71, 1197-1213, DOI: 10.1016/j.gca.2006.11.031.

40. Buczynski, C.; Chafetz, H.S. Habit of bacterially induced precipitates of calcium carbonate and the influence of medium viscosity on mineralogy. *Journal of Sedimentary Research*, **1991**, 61, 226-233.
41. Zhuang, D.; Yan, H.; Tucker, M. E. Calcite precipitation induced by Bacillus cereus MRR2 cultured at different Ca^{2+} concentrations: Further insights into biotic and abiotic calcite. *Chemical Geology*, **2018**. DOI:10.1016/j.chemgeo.2018.09.018
42. Grasby, S.E. Naturally precipitating vaterite (μ-CaCO3) spheres: unusual carbonates formed in an extreme environment. *Geochimica et Cosmochimica Acta*, **2003**, 67, 1659-1666.
43. Wei, S.; Cui, H.; Jiang, Z. Biomineralization processes of calcite induced by bacteria isolated from marine sediments. *Brazilian Journal of Microbiology*, **2015**, 46, 455-464. DOI: 10.1590/S1517-838246220140533.
44. Sánchez-Román, M.; Rivadeneyra, M. A.; Vasconcelos, C. Biomineralization of carbonate and phosphate by moderately halophilic bacteria. *FEMS Microbiology Ecology*, **2007**, 61, 273-284. DOI: 10.1111/j.1574-6941.2007.00336.x
45. Teng, H.H.; Dove, P.M.; Deyoreo, J.J. Reversed calcite morphologies induced by microscopic growth kinetics: insight into biomineralization. *Geochimica et Cosmochimica Acta*, **1999**, 63, 2507-2512. DOI: 10.1016/S0016-7037(99)00103-9
46. Addadi, L.; Weiner, S. Interactions Between Acidic Macromolecules and Structured Crystal Surfaces Stereochemistry and Biomineralization. *Molecular Crystals*, **1986**, 134, 305-322. DOI: 10.1016/j.msec.2005.01.003
47. Rusznyák, A.; Akob, D.M.; Nietzsche, S. Calcite biomineralization by bacterial isolates from the recently discovered pristine karstic Herrenberg cave. *Appl Environ Microbiol*, **2012**, 78, 1157-1167.
48. Kalmar, L.; Homola, D.; Varga, G. Structural disorder in proteins brings order to crystal growth in biomineralization. *Bone*, **2012**, 51, 528-534, DIO: 10.1016/j.bone.2012.05.009
49. Teng, H.H.; Dove, P.M. Surface site-specific interactions of aspartate with calcite during dissolution; implications for biomineralization. *American Mineralogist*, **1997**, 82, 878-887, DOI: 10.2138/am-1997-9-1005
50. Marin, F.; Luquet, G. Molluscan biomineralization: The proteinaceous shell constituents of Pinna nobilis L. *Materials Science & Engineering*, **2005**, 25, 105-111, DOI: 10.1016/j.msec.2005.01.003.
51. Sánchez-Román, M.; Romanek, C.S.; Fernández-Remolar, D.C. Aerobic biomineralization of Mg-rich carbonates: Implications for natural environments. *Chemical Geology*, **2011**, 281, 143-150, DOI: 10.1016/j.chemgeo.2010.11.020.
52. Couradeau, E.; Benzerara, K.; Gérard, E. An early-branching microbialite cyanobacterium forms intracellular carbonates. *Science*, **2012**, 336, 459. DOI: 10.1126/science.1216171
53. Benzerara, K.; Skouripanet, F.; Li, J. Intracellular Ca-carbonate biomineralization is widespread in cyanobacteria. *Proceedings of the National Academy of Science of the United States of America*, **2014**, 111, 10933-10938. DOI: 10.2307/23804968
54. Chen, Y.; Meng, Q.; Liu, S.Y. Durable antimicrobial finishing of cellulose with QSA silicone by supercritical adsorption, *Applied Surface Science*, **2013**, 264, 171-175. DOI: 10.1016/j.apsusc.2012.09.165
55. Liu, Q.Y.; Zhu, J.Q.; Sun, T. Porphyrin nanotubes composed of highly ordered molecular arrays prepared by anodic aluminum template method, *RSC Advances*, **2013**, 3, 2765-2769. DOI: 10.1039/c2ra21364h

56. Zhou, S.X.; Chen H.P.; Ding, C.; Yu, H.G. Effectiveness of crystallitic carbon from coal as milling aid and for hydrogen storage during milling with magnesium, *Fuel*, **2013**, 109, 68-75. DOI: 10.1016/j.fuel.2012.09.002
57. Zhou, S.X.; Chen H.P.; Wang,N.F.; Han, Z.Y. Effect of carbon from anthracite coal on decomposition kinetics of magnesium hydride, *Journal of Alloys and Compounds*, **2014**, 592, 231-237. DOI: 10.1016/j.jallcom.2013.12.246
58. Wang, J.J.; Wang, J.Q.; Lu, J.M.; Yang, J.H. Hollow mesoporous silica spheres synthesized with cationic and anionic mixed surfactant as templates, *Materials letters*, **2015**, 142, 269-272. DOI: 10.1016/j.matlet.2014.11.092
59. Huang, Y.Q.; Zhao, Q.; Wang, Y.H. A New Layered Six-Connected Network Based on Tetranuclear Copper (II) Cores. *Journal of Chemical Crystallography*, **2012**, 42, 706-710. DOI: 10.1007/s10870-012-0304-y
60. Zhao, B.; Shao, Q.; Hao, L. Yeast-template synthesized Fe-doped cerium oxide hollow microspheres for visible photodegradation of acid orange 7. *Journal of colloid and interface science*, **2018**, 511, 39-47. DOI: 10.1016/j.jcis.2017.09.077
61. Hu, X.; Cheng, W.; Shao, Z. Synthesis and characterization of temperature-sensitive hydrogels. *e-Polymers*, **2015**, 15, 353-360. DOI: 10.1515/epoly-2015-0157
62. Hu, X.; Cheng, W.; Shao, Z. Novel authigenic gas foaming hydrogels for preventing coal spontaneous combustion. *e-Polymers*, **2015**, 15，361-368. DOI: 10.1515/epoly-2015-0156
63. Wu, T.; Shao, Q.; Ge, S. The facile preparation of novel magnetic zirconia composites with the aid of carboxymethyl chitosan and their efficient removal of dye. *RSC Advances*, **2016**, 6, 58020-58027. DOI: 10.1039/c6ra05273h
64. Ma, Y.; Lv, L.; Guo, Y. Porous lignin based poly (acrylic acid)/organo-montmorillonite nanocomposites: swelling behaviors and rapid removal of Pb (II) ions. *Polymer*, **2017**, 128，12-23. DOI: 10.1016/j.polymer.2017.09.009
65. Huang, J.; Cao, Y.; Shao, Q. Magnetic nanocarbon adsorbents with enhanced hexavalent chromium removal: morphology dependence of fibrillar vs particulate structures. *Industrial and Engineering Chemistry Research*, **2017**, 56, 10689-10701. DOI: 10.1021/acs.iecr.7b02835
66. Wu, Z.; Gao, S.; Chen, L. Electrically insulated epoxy nanocomposites reinforced with synergistic core–shell SiO_2@ MWCNTs and montmorillonite bifillers. *Macromolecular Chemistry and Physics*, **2017**, 218, 1700357. DOI: 10.1002/macp.201700357
67. Zhu, W.; Ge, S.; Shao, Q. Adsorption properties of ZrO_2 hollow microboxes prepared using $CaCO_3$ cubes as templates. *RSC Advances*, **2016**, 6, 81736-81743. DOI: 10.1039/c6ra11639f
68. Hu, X.; Cheng, W. Synthesis and characterization of a temperature-sensitive hydrogel based on sodium alginate and N-isopropylacrylamide. *Polymers for Advanced Technologies*, **2015**, 26, 1340-1345. DOI: 10.1002/pat.3682
69. Zhao J, Ge S, Liu L, et al. Microwave solvothermal fabrication of zirconia hollow microspheres with different morphologies using pollen templates and their dye adsorption removal. *Industrial and Engineering Chemistry Research*, **2017**, 57, 231-241. DOI: 10.1021/acs.iecr.7b04000
70. Liu, Q.Y.; Jia, Q.Y.; Zhu, J.Q. Highly ordered arrangement of meso-tetrakis (4-aminophenyl) porphyrin in self-assembled nanoaggregates via hydrogen bonding. *Chinese Chemical Letters*, **2014**, 25, 752-756. DOI: 10.1016/j.cclet.2013.12.023

71. Wu, T.; Shao, Q.; Ge, S. The facile preparation of novel magnetic zirconia composites with the aid of carboxymethyl chitosan and their efficient removal of dye. RSC Advances, 2016, 6, 58020-58027. DOI：10.1039/C6RA05273H

72. Ge, S. Zhu, W. Shao, Q. Fabrication and characterization of hollow zirconia microspheres using calcium carbonate as template. *Zeitschrift für Physikalische Chemie*, **2016**, 230, 1617-1628. DOI: 10.1515/zpch-2015-0681

73. Liu, X.; Shao, X. Y. Fang, G.B. Preparation and properties of chemically reduced graphene oxide/copolymer-polyamide nanocomposites. *e-Polymers*, **2017**, 17, 3-14. DOI: 10.1515/epoly-2016-0094

74. Tian, J.; Shao, Q.; Dong, X. Bio-template synthesized NiO/C hollow microspheres with enhanced Li-ion battery electrochemical performance. *Electrochimica Acta*, **2018**, 261: 236-245. DOI：10.1016/j.electacta.2017.12.094

75. Huang, J.; Cao, Y.; Shao, Q. Magnetic nanocarbon adsorbents with enhanced hexavalent chromium removal: morphology dependence of fibrillar vs particulate structures. *Industrial and Engineering Chemistry Research*, **2017**, 56, 10689-10701. DOI： 10.1021/acs.iecr.7b02835

76. Ge, S.S.; Yang,X.k.; Shao, Q.; Liu ,Q.Y. Self-assembled flower-like antimony trioxide microstructures with high infrared reflectance performance, *Journal of Solid State Chemistry*, **2013**, 200, 136-142. DOI: 10.1016/j.jssc.2013.01.027

77. Liu, Q.; Zhao, Q.; Li, Y. $CdCl_2 \cdot H_2O$ nanorods oriented parallel on the langmuir film of (Phthalocyaninato) [Tetrakis(4-pyridyl)porphyrinato] cerium complex. *CrystEngComm*, **2012**, 14, 1105-1110. DOI: 10.1039/c1ce05702b

78. Liu, Q.Y.; Yang, Y.T.; Li, H.; Zhu,R.R.; NiO nanoparticles modified with 5,10,15,20-tetrakis(4-carboxyl pheyl)-porphyrin: Promising peroxidase mimetics for H_2O_2 and glucose detection. *Biosensors and Bioelectronics*, **2015**, 64, 147-153. DOI: *10.1016/j.bios.2014.08.062*

79. He, M.; Jin, H.; Zhang, L.; Jiang, H.; Yang, T.; Cui, H. Environmental transmission electron microscopy investigations of Pt-Fe_2O_3 nanoparticles for nucleating carbon nanotubes. *Carbon*, **2016**, 110, 243-248. DOI: 10.1016/j.carbon.2016.09.026

80. Zhao, H.; Yan, H.; Zhang, C.; Sun, B. Thermogravimetry study of pyrolytic characteristics and kinetics of the giant wetland plant Phragmites australis. *Journal of Thermal Analysis and Calorimetry*, **2012**, 110, 611-617. DOI: 10.1007/s10973-011-2018-3

81. Tian, B.; Qiao, Y.; Tian, Y. FTIR study on structural changes of different–rank coals caused by single/multiple extraction with cyclohexanone and NMP/CS2 mixed solvent. *Fuel Processing Technology*, **2016**, 154,210-218. DOI: ： 10.1016/j.fuproc.2016.08.035

82. Wang, J.; Chen, D.; Xu, Y. Influence of the crystal texture on Raman spectroscopy of the AlN films prepared by pulse laser deposition. *Journal of Spectroscopy*, 2012, DOI: 10.1155/2013/103602

83. Sánchez-Román, M.; Romanek, C. S.; Fernández-Remolar, D.C. Aerobic biomineralization of Mg-rich carbonates: Implications for natural environments. *Chemical Geology*, **2011**, 281, 143-150. DOI: 10.1016/j.chemgeo.2010.11.020

84. Sültemeyer, D.; Schmidt, C.; Fock, H.P. Carbonic anhydrases in higher plants and aquatic microorganisms. *Physiologia Plantarum*, **1993**, 88, 179–190, DOI: 10.1034/j.1399-3054.1993.880125.x.

85. Achal, V.; Pan, X.; Characterization of urease and carbonic anhydrase producing bacteria and their role in calcite precipitation. *Current Microbiol*. **2011**, 62, 894–902, DOI: 10.1007/s00284-010-9801-4.
86. Scozzafava, A.; Supuran, C.T. Hydroxyurea is a carbonic anhydrase inhibitor. *Bioorganic and medicinal chemistry*, **2003**, 11, 2241-2246, DOI: 10.1016/S0968-0896(03)00112-3.
87. Lindskog, S. Structure and mechanism of carbonic anhydrase. *Pharmacol Ther*, **1997**, 74, 1-20.
88. Hermann, G.J.; Thatcher, J.W.; Mills, J.P. Mitochondrial fusion in yeast requires the transmembrane GTPase Fzo1p. *Journal of cell biology*, **1998**, 143, 359-373. DOI: 10.1083/jcb.143.2.359
89. Dhami, N.K.; Mukherjee, A.; Reddy, M.S. Micrographical, minerological and nano-mechanical characterisation of microbial carbonates from urease and carbonic anhydrase producing bacteria. *Ecological Engineering*, **2016**, 94, 443-454, DOI: 10.1016/j.ecoleng.2016.06.013.
90. Albeck, S.; Aizenberg, J.; Addadi, L., Weiner, S. Interactions of various skeletal intracrystalline components with calcite crystals. Journal of the American Chemical Society, 115, 11691-11697. DOI: 10.1021/ja00078a005
91. Albeck, S.; Addadi, L.; Weiner, S. Regulation of calcite crystal morphology by intracrystalline acidic proteins and glycoproteins. *Connect Tissue Research*. **1996**, 35, 419-424. DOI: 10.3109/03008209609029213
92. Albeck, S.; Weiner, S.; Addadi, L. b. Polysaccharides of intracrystalline glycoproteins modulate calcite crystal growth in vitro. *Chenistry-a European Journal*, **1996**, 2, 278-284. DOI: 10.1002/chem.19960020308
93. Lowenstam, H.A.; Weiner, S. On biomineralization. *Oxford University Press on Demand*, **1989**.
94. Aizenberg, J.; Hanson, J.; Koetzle, T. F.; Weiner, S.; Addadi, L. Control of macromolecule distribution within synthetic and biotic single calcite crystals. *Journal of the American Chemical Society*, **1997**, 119, 881-886. DOI: 10.1021/ja962882
95. Aizenberg, J.; Lambert, G.; Weiner, S.; Addadi, L. Factors involved in the formation of amorphous and crystalline calcium carbonate: a study of an ascidian skeleton. *Journal of the American Chemical Society*, **2002**, 124, 32-39. DOI: 10.1021/ja016990l
96. Wang, Y.Y.; Yao, Q.Z.; Zhou, G.T. Formation of elongated calcite mesocrystals and implication for biomineralization. *Chemical Geology*, **2013**, 360–361, 126-133, DOI: 10.1016/j.chemgeo.2013.10.013.
97. Seifan, M.; Samani, A.K.; Berenjian, A. Induced calcium carbonate precipitation using Bacillus species. *Applied microbiology and biotechnology*, **2016**, 100, 9895-9906. DOI: 10.1007/s00253-016-7701-7
98. Tourney, J.; Ngwenya, B.T. Bacterial extracellular polymeric substances (EPS) mediate CaCO3 morphology and polymorphism. *Chemical Geology*, **2009**, 262, 138-146, DOI: 10.1016/j.chemgeo.2009.01.006.
99. Bendinger, B.; Rijnaarts, H.H.; Altendorf, K. Physicochemical cell surface and adhesive properties of coryneform bacteria related to the presence and chain length of mycolic acids. *Applied and Environmental Microbiology*, **1993**, 59, 3973-3977.
100. Rodriguez-Navarro, C.; Jimenez-Lopez, C.; Rodriguez-Navarro, A. Bacterially mediated mineralization of vaterite. *Geochimica et Cosmochimica Acta*, **2007**, 71, 1197-1213, DOI: 10.1016/j.gca.2006.11.031.

101. Tourney, J.; Ngwenya, B.T.; Mosselmans, J.W. Physical and chemical effects of extracellular polymers (EPS) on Zn adsorption to Bacillus licheniformis S-86. *Journal of Colloid and Interface Science*, **2009**, 337, 381, DOI: 10.1016/j.jcis.2009.05.067.
102. Jiang, W.; Saxena, A.; Song, B. Elucidation of functional groups on gram-positive and gram-negative bacterial surfaces using infrared spectroscopy. *Langmuir*, **2004**, 20, 11433-11442, DOI: 10.1021/la049043+.
103. Lev, S.; Moreno, H.; Martinez, R. Protein tyrosine kinase PYK2 involved in Ca^{2+}-induced regulation of ion channel and MAP kinase functions. *Nature*, ***1995***, 376, 737-745.
104. Urzi, C.; Garcia-Valles, M.; Vendrell, M. Biomineralization processes on rock and monument surfaces observed in field and in laboratory conditions. *Geomicrobiology*, 1999, 16, 39-54, DOI: 10.1080/014904599270730.
105. Xu, J.; Wang, J.; Hong, M. Solution-chemistry control of Mg^{2+}-calcite interaction mechanisms: Implication for biomineralization. *American Mineralogist*, **2016**, 101, 1104-1112. DOI: 10.2138/am-2016-5406
106. Lowenstein, T.K.; Timofeeff, M.N.; Brennan, S.T.; Hardie, L.A.; Demicco, R.V. Oscillations in Phanerozoic seawater chemistry: evidence from fluid inclusions. *Science*, **2001**, 294, 1086–1088.DOI: 10.1126/science.1064280
107. Horita, J.; Zimmermann, H.; Holland, H.D. Chemical evolution of seawater during the Phanerozoic: Implications from the record of marine evaporites. *Geochimica et Cosmochimica Acta*, **2002**, 66, 3733–3756, DOI: 10.1016/S0016-7037(01)00884-5
108. Timofeeff, M.N.; Lowenstein, T.K. Secular variation in the major-ion chemistry of seawater: Evidence from fluid inclusions in Cretaceous halites. *Geochimica et Cosmochimica Acta*, **2006**, 70, 1977–1994. DOI: 10.1016/j.gca.2006.01.020
109. Ries, J.B. Geological and experimental evidence for secular variation in seawater Mg/Ca (calcite-aragonite seas) and its effects on marine biological calcification. Biogeosciences, 2010, 7(9): 2795.
110. Ries, J.B.; Anderson, M.A.; Hill, R.T. Seawater Mg/Ca controls polymorph mineralogy of microbial CaCO3: A potential proxy for calcite-aragonite seas in Precambrian time. *Geobiology*, **2008**, 6, 106-119. DOI: 10.1111/j.1472-4669.2007.00134.x
111. Xu, J.; Yan, C.; Zhang, F. Testing the cation-hydration effect on the crystallization of Ca–Mg–CO3 systems. *Proceedings of the National Academy of Sciences*, **2013**, 110, 17750-17755. DOI: 10.2307/23754384
112. Catterall, W.A. Structure and regulation of voltage-gated Ca2+ channels. *Annual review of cell and developmental biology*, **2000**, 16, 521-555.DOI: 10.1146/annurev.cellbio.16.1.521
113. Miedema, H.; Meter-Arkema, A.; Wierenga, J. Permeation properties of an engineered bacterial OmpF porin containing the EEEE-locus of Ca^{2+} channels. *Biophysical Journal*, **2004**, 87, 3137-3147. DOI: 10.1529/biophysj.104.041384
114. Moomaw, A.S.; Maguire, M.E. Cation selectivity by the CorA Mg^{2+} channel requires a fully hydrated cation. Biochemistry, 2010, 49, 5998-6008. DOI: 10.1021/bi1005656
115. Dudev, T.; Lim, C. Competition among Ca^{2+}, Mg^{2+}, and Na^{+} for model ion channel selectivity filters: determinants of ion selectivity. *The journal of physical chemistry B*, **2012**, 116, 10703-10714. DOI: 10.1021/jp304925a

116. Van, Lith.Y.; Warthmann,R.; Vasconcelos, C. Microbial fossilization in carbonate sediments: a result of the bacterial surface involvement in dolomite precipitation. *Sedimentology*, **2003**, 50, 237-245. DOI: 10.1046/j.1365-3091.2003.00550.x

117. Sánchez-Román, M.; Vasconcelos, C. Schmid, T. Aerobic microbial dolomite at the nanometer scale: Implications for the geologic record. *Geology*, **2008**, 36, 879-882. DOI: 10.1130/G25013A.1

118. Bontognali, T.R.R.; Vasconcelos, C.; Warthmann, R.J. Microbes produce nanobacteria-like structures, avoiding cell entombment. *Geology*, **2008**, 36, 663-666. DOI: 10.1130/G24755A.1

119. Bontognali, T.R.R.; Vasconcelos, C.; Warthmann, R.J. Dolomite formation within microbial mats in the coastal sabkha of Abu Dhabi (United Arab Emirates). *Sedimentology*, **2010**, 57, 824-844. DOI: 10.1111/j.1365-3091.2009.01121.x

120. Perri, E.; Tucker, M.E.; Słowakiewicz, M.; Whitaker, F.; Bowen, L.; Perrotta, I.D. Carbonate and silicate biomineralization in a hypersaline microbial mat (Mesaieed sabkha, Qatar): Roles of bacteria, extracellular polymeric substances and viruses. *Sedimentology*. **2017**. 65, 1213-1245. DOI: 10.1111/sed.12419